Cretaceous Research 146 (2023) 105464

Contents lists available at ScienceDirect

Cretaceous Research

journal homepage: www.elsevier.com/locate/CretRes

Timing of the Greenhorn transgression and OAE2 in Central Utah using CA-TIMS U-Pb zircon dating

Ray K. Renaut [a,*], Ryan T. Tucker [a], M. Ryan King [b], James L. Crowley [c], Ethan G. Hyland [d], Lindsay E. Zanno [e,f]

[a] Department of Earth Sciences, Faculty of Science, University of Stellenbosch, Private Bag X1, Matieland 7602, South Africa
[b] Department of Natural and Environmental Sciences, Western Colorado University, 1 Western Way, Gunnison, CO 81231, USA
[c] Department of Geosciences, Boise State University, Boise, ID 83725, USA
[d] Department of Marine, Earth, and Atmospheric Sciences, 2800 Faucette Dr., North Carolina State University, Raleigh, NC 27695, USA
[e] Paleontology, North Carolina Museum of Natural Sciences, 11 W. Jones St., Raleigh, NC 27601, USA
[f] Department of Biological Sciences, Campus Box 7617, North Carolina State University, Raleigh, NC, 27695, USA

ARTICLE INFO

Article history:
Received 18 May 2022
Received in revised form
10 November 2022
Accepted in revised form 29 December 2022
Available online 24 January 2023

Keywords:
TT1
TT4
Ash Fall
Naturita Sandstone
Tununk Shale
CA-TIMS

ABSTRACT

Contextualizing subbasinal influences on accommodation and pace of the rapid landscape evolution during the base-level rise of the Upper Cretaceous (upper Cenomanian–lower Turonian) Greenhorn Cycle within the Western Interior of North America requires refined stratigraphic controls of key sediment successions. Herein, a blended analysis of laser ablation inductively coupled plasma mass spectrometry (LA-ICP-MS), chemical abrasion thermal ionization mass spectrometry (CA-TIMS), and $\delta^{13}C$ isotopic data is utilized to identify two regionally significant ash-fall marker beds southeast of the Wasatch Plateau, specifically the TT1 and TT4, which bracket the Cenomanian–Turonian boundary and the Greenhorn Cycle transgression in the Western Interior Seaway (WIS). Based on our analysis of the recovered ash-fall zircons, a meaningful depositional age (DA) for the TT1 is 94.616 Ma ± 0.027 and 94.010 Ma ± 0.017 for the TT4 bentonite of the Tununk Shale.

When coupled with the pre-existing biostratigraphic framework, correlation potential greatly increases with the (TT1) Naturita falling within the *Sciponoceras gracile* Assemblage Zone. Common molluscs associated with this biozone within the southern and central regions of Utah include *Inoceramus pictus*, *Euomphaloceras* spp., and *Pycnodonte newberryi*. The (TT4) Tununk within the upper portion of the *Watinoceras coloradoense* Assemblage Zone is commonly associated with the following mollusc genus within the areas to the south and north of the study area: *Mytiloides* and *Morrowites*. Furthermore, these dates constrain the Cenomanian–Turonian boundary, provide accurate chronostratigraphic markers for intra and interbasinal correlation and serve to strengthen global linkages to Ocean Anoxic Event 2 (OAE2) during the Greenhorn Cycle transgression.

1. Introduction

Late Cenomanian changes in oxygen content of oceanic waters as a result of the northward incursion of warm Tethyan water into the Western Interior Seaway (WIS) during the early Greenhorn Cycle transgression triggered a notable increase in the preserved diversity of micro and macrofauna (Cobban and Reeside, 1952; Kauffman, 1977; Eicher and Diner, 1985; Elder, 1987, 1989; Caldwell et al., 1993; Watkins et al., 1993; Leckie et al., 1998; Eldrett et al., 2014; Elderbak and Leckie, 2016; Lowery et al., 2017; O'Connor et al., 2020). This may be attributed to re-oxygenation of the WIS, in particular the “Benthonic Zone” (Eicher and Worstell, 1970), as well as the migration of marine species associated with the incursion of low latitude water masses into the WIS (Eicher and Diner, 1985; Elder, 1987; Caldwell et al., 1993; Kauffman and Caldwell, 1993; Leckie et al., 1998; Elderbak and Leckie, 2016) and demarcates the initial bulk oxygen-isotope excursion, roughly ~94 Ma (van Helmond et al., 2015; van Helmond et al., 2016; Eldrett et al., 2017; Lowery et al., 2018; O'Connor et al., 2020). Thereafter, progressive geochemical shifts to more reducing conditions changed the geographical and temporal distribution as well as the diversity

* Corresponding author.
E-mail address: 24652687@sun.ac.za (R.K. Renaut).

https://doi.org/10.1016/j.cretres.2022.105464

of both benthic and planktic micro and macrofaunal assemblages (Elder, 1987, 1991; Eldrett et al., 2014; Eldrett et al., 2017; Boudinot et al., 2020; Bryant et al., 2021; Forkner et al., 2021). This contributed significantly to changes in the accumulations of organic material emplaced on the seafloor, providing valuable information regarding local and regional changes in oxygen content, as well as the vertical and horizontal extent of local and regional water column stratification during the Greenhorn transgression (Elder, 1991; Meyers et al., 2005; Turgeon and Creaser, 2008; van Helmond et al., 2015; Elderbak and Leckie, 2016; van Helmond et al., 2016; Eldrett et al., 2017; Boudinot et al., 2020). These transitions in faunal assemblages have been associated temporally with the presence of an astrogeochronologically determined 300–980 kyr global Oceanic Anoxic Event 2 (OAE2) (Sageman et al., 1997; Meyers et al., 2001; Sageman et al., 2006; Laurin and Sageman, 2007; Meyers et al., 2012; Eldrett et al., 2015; Jones et al., 2018; Jones et al., 2019; Jones et al., 2021) and coincides with a major, stepwise marine-based extinction event at or near the C–T boundary (Elder, 1985, 1989, 1991; Kauffman et al., 1993; Eaton et al., 1997; Harries and Little, 1999; Forkner et al., 2021). Consequently, the OAE2 provides a globally significant boundary marker combining key faunal shifts with resulting changes in lithology and organic content levels (positive δ13C excursion) (Schlanger and Jenkyns, 1976; Arthur et al., 1987; Tsikos et al., 2004; Turgeon and Creaser, 2008; Eldrett et al., 2014; van Helmond et al., 2015; van Helmond et al., 2016; Eldrett et al., 2017; O'Connor et al., 2020). Therefore, with the general global absence of key ash bed dates for geochronological correlation, the C–T boundary in the WIS is identified by global shifts in faunal occurrences such as the: 1) first occurrence of *Watinoceras devonense* Wright and Kennedy (1981); 2) diversification of the genus *Mytiloides* Brongniart (Deville, 1989); and 3) the last occurrence of the key mollusc *Inoceramus pictus* Sowerby (1829) (Kennedy et al., 2005).

The aforementioned events have contributed significantly to the temporal and geographical distribution of species within the marine sedimentary successions of the Upper Cretaceous of the WIS (Warren and Stelck, 1969; Cobban and Scott, 1972; Kirkland, 1991; Kauffman et al., 1993; Cobban et al., 2006; Merewether et al., 2011; Walaszczyk et al., 2014; and references therein). Identification of these successions, and the associated faunal turnover, has resulted in the development of marine molluscan biozonation which was vital in the initial, as well as present, correlation of strata across the Cretaceous WIS (Warren and Stelck, 1969; Cobban and Scott, 1972; Kirkland, 1991; Kauffman et al., 1993; Cobban et al., 2006; Merewether et al., 2011; Walaszczyk et al., 2014; and references therein). Although more continuous in terms of lithological and biological preservation, unique complications exist in refining the stratigraphy of these marine sediments in the WIS during the late Cenomanian–early Turonian, such as the scarcity or absence of ammonites related to the OAE's in sediments approaching stage boundaries (Elder, 1989, 1991). In addition, the first and last occurrence of various ammonites, such as the first occurrence of the upper Cenomanian *Sciponoceras gracile* Shumard (1860), may correlate to significant geological events such as the onset of the OAE2 (Jones et al., 2019; Boudinot et al., 2020). However, extensive temporal distribution overlapping into other biozones may reveal that these taxa are not suitable as the index species of a previously defined taxon-range biozone (Cobban et al., 2006; Dodsworth and Eldrett, 2019). Limitations of microfossil biostratigraphic correlation include: 1) preservational bias (Desmares et al., 2007); 2) coarse stratigraphic ranges for many forms, including palynomorphs, dinocysts, and acritarchs (Dodsworth and Eldrett, 2019); and 3) diachroneity of bases of biozones due to migration in marine environments of dinoflagellate cysts at different geological times, associated with the movement of water masses from the southerly based Tethyan sea northwards into the WIS (Dodsworth and Eldrett, 2019).

More recently, many of these tenuous biostratigraphic linkages have been calibrated by absolute age dating to increase stratigraphic resolution. Furthermore, temporally anchoring key Age/Stage boundaries with absolute dates (Ar–Ar or U–Pb), particularly regarding the Cenomanian–Turonian transition, remains an ongoing process (Gradstein and Ogg, 2004; Meyers et al., 2012; Ogg and Hinnov, 2012; Eldrett et al., 2015; Laurin et al., 2019; Jones et al., 2021). Differences in biozone markers across terrestrial and marine strata, coupled with different methods used to attain radiometric age dates (Ar–Ar or U–Pb) for these strata, add difficulty to calibrating this global event locally and regionally (Obradovich, 1993; Gradstein et al., 2004; Kennedy et al., 2005; Cobban et al., 2006; Meyers et al., 2012; Ogg and Hinnov, 2012; Jones et al., 2019). In this regard, there are four regionally correlated bentonite marker beds, TT1–TT4 (the bentonite marker beds "A–D" of Elder (1985, 1988); "PBC-5, PBC-11, PBC-17, PBC-20" of Elder and Kirkland (1985), Elder (1988), Kowallis et al. (1989); Kowallis et al. (1995) and "T1–T4" of Zelt (1985) and Li and Schieber (2018)), in central and southern Utah that temporally constrain Cenomanian–Turonian biozones within the Sevier Foreland Basin. The C–T boundary is specifically bracketed between TT2–TT3 (Leithold, 1993; Sethi and Leithold, 1997; Tibert et al., 2003; Tibert and Leckie, 2013). Early attempts, using uncalibrated $^{40}Ar–^{39}Ar$ (sanidine) dating techniques to temporally constrain TT2 to TT3, yielded generally younger approximate age ranges of 93.5–93.0 Ma for the boundary (Obradovich, 1993; Kowallis et al., 1995; Gradstein and Ogg, 2004; Cobban et al., 2006). Recalibration of these aforementioned age ranges through the use of the Fish Canyon sanidine standard age, as well as using alternative methods such as U–Pb (zircon) radiometric dating, has indicated overall that the temporal placement of the C–T boundary is more likely to have occurred closer to 94 Ma (Meyers et al., 2012; Ogg and Hinnov, 2012; Eldrett et al., 2015; Laurin et al., 2019; Jones et al., 2019). Notwithstanding these challenges, radiometric age dates are invaluable for resolving pervasive inconsistencies in correlating and temporally constraining both marine and continental strata within the Western Interior Basin (WIB) (Cifelli et al., 1997, 1999; D'Emic et al., 2019; Miall and Catuneanu, 2019; Nesbitt et al., 2019; Zanno et al., 2019).

Here we assess the first ash-fall U–Pb zircon age dates (via CA-TIMS and LA-ICP-MS) from the northern Last Chance Desert, south of the Wasatch Plateau, Central Utah, providing DA's for individual ash falls deposited within the Naturita Sandstone and Tununk Shale, whilst simultaneously providing regional linkages via the TT1 and TT4a (lower doublet) respectively. These new-age data, correlated to local δ13C excursion data analyzed in this paper, allow us to refine temporal correlation of the Western Interior Sea Level Curves (flooding surface) further via ashfall DA's; place diachronous transgressive surfaces into a more constrained chronostratigraphic framework across lateral basins in the region; and discern any possible relationships between volcanism and sedimentation. These new data will also provide more robust linkages between key strata across the whole of the Western Interior during the transition from the Greenhorn transgression and allow for correlation with time equivalent continental successions.

2. Geological background

Initially formed as an expansive foreland basin, the WIB is preserved within a mosaic of subbasins as a consequence of orogenic events (155–35 Myr) (Greenhalgh and Britt, 2007; Roca and Nadon, 2007). Later phases of this deformation included the thin-skinned Sevier fold-thrust belt and the younger basement-core uplifts of the Laramide Orogeny (Willis, 1999). Of particular relevance to this study is the coeval thrust-load (Pavant Thrust), which generated flexural subsidence associated with deformation in the Sevier Thrust Belt (Currie, 2002). Resulting eastward migration of the flexural domains lead to the emplacement of sediments of the uppermost Cedar Mountain Formation, as well as the Naturita Sandstone and the Tununk Shale during the early Cenomanian to early Turonian foredeep (Currie, 1997; White et al., 2002; Miall et al., 2008).

2.1. Naturita Sandstone

Herein, we agree with Carpenter's (2014) reiteration of Young (1960, 1965) that the Naturita is lithostratigraphically composed of strata along the western shoreline of the WIS sourced by the Sevier Orogeny and Dakota strata conversely lies along the eastern shoreline sourced from the North American Craton. For clarity, given that our study area lies within the western confines of the Colorado Plateau, we refer to Carpenter (2014), and therefore, the unit overlying the Cedar Mountain Formation is identified as the Naturita Sandstone and not Naturita (Dakota), Dakota Sandstone or Dakota Formation (Barclay et al., 2015; Laurin et al., 2019).

Regionally, the cliff-forming Naturita unconformably overlies the Mussentuchit Member of the Cedar Mountain Formation (Figs. 1, 2) (Eaton et al., 1990; Currie, 1997; Phillips et al., 2020; Tucker et al., 2020, Tucker et al., 2022) with observable undercutting by the Naturita into this lower stratum reported by several authors within the study area (Eaton et al., 1990; Phillips et al., 2020; Tucker et al., 2020; and references therein). The laterally discontinuous deposits of the Naturita form a complex combination of mudstone, shale and carbonaceous units with distinctly positioned fossiliferous conglomerates which are indicative of continental provenance as well as marine origins (Young, 1965; Eaton et al., 1990; Kirschbaum and Schenk, 2010; Kirkland et al., 2016; Phillips et al., 2020). Thus, the stratigraphy of the Naturita provides a sequence documenting the transformation of a largely inland fluvial to a marine environment. The final transgressive lag deposits of the Naturita are overlain by the offshore mudstones characteristic of two geographically separated basal members of the Mancos Shale: the Tropic Shale of the Markagunt, Paunsaugunt and Kaiparowits Plateaus (Zelt, 1985; Leithold, 1994; Eaton et al., 2001; Tibert et al., 2003; Tibert and Leckie, 2013; Jones et al., 2019) and the Tununk Shale of the Henry Mountain Basin and the Wasatch Plateau (Zelt, 1985; Eaton et al., 1990; Leithold, 1994; Tibert et al., 2003; Kirschbaum and Schenk, 2010; Tibert and Leckie, 2013; Carpenter, 2014; Phillips et al., 2020). The top of the Naturita is marked by an ash in the study area (interpreted to be TT2 herein, measured section Fig. 2) and then within a meter is capped with a transgressive erosional deposit containing the molluscan bivalve *Pycnodonte newberryi* Stanton (1893). An unconformity exists between the Tununk Shale and either the uppermost Naturita (Eaton et al., 1990 “Dakota Formation”; Molenaar and Cobban, 1991 “Dakota Formation”; Gardner, 1995 “Dakota Formation”; Carpenter, 2014; Phillips et al., 2020) or Cedar Mountain Formation (Eaton et al., 1990) in the central, northeastern and eastern regions of Utah.

2.2. Tununk Shale

The Tununk Shale, deposited on the western side of the WIS, is the lowest member of the Mancos Shale and, depending on its geographic occurrence in Utah and Colorado, overlies either the Naturita (Zelt, 1985 “Dakota Formation”; Leithold, 1993, 1994 “Dakota Formation”; Li and Schieber, 2018, 2020 “Dakota Formation”Carpenter, 2014; Phillips et al., 2020) or the Cedar Mountain Formation (Eaton et al., 1990; Molenaar and Cobban, 1991; and references therein). This particular marine sedimentary succession accumulated on a storm-dominated, offshore shelf (Li and Schieber, 2018) to pro-deltaic environment (Leithold and Dean, 1998; and references therein) and are correlated across the southern-central and central to eastern parts of Utah (Zelt, 1985; Leithold, 1993, 1994; Li and Schieber, 2018). One of these ash beds, interpreted as TT2, and the overlying *P. newberryi*-bearing transgressive lag marks the transition to the Tununk. As discussed in Section 2.1, an observable unconformity exists between the Naturita and the Tununk at the study locality.

Progressing from the base of the Tununk, the sediment generally coarsens upwards, with the contact between the overlying paralic sediments of the Ferron Sandstone described by Molenaar and Cobban (1991) as a gradational conformity on the western side of the San Rafael uplift although a moderately thick volcanic ash has been observed between these two units in certain areas of the San Rafael area (Rigby et al., 1987). Gardner (1995) notes the presence of a paraconformity in the northern Castle Valley region.

2.3. Ashbeds TT1 and TT4

Regionally, the TT1 occurs within the Naturita Sandstone, Tropic Shale or Tununk Shale in the southern to central regions of Utah (Fig. 3), and is equivalent to: 1) the bentonite marker beds “A” of Elder (1985; 1987); 2) PBC-5 of Elder and Kirkland (1985), Kowallis et al. (1989) and Kowallis et al. (1995); 3) T1 of Zelt (1985) and Li and Scheiber (2018); 4) is generally positioned near to the base of the *Sciponoceras gracile*/*Euomphaloceras septemseriatum* biozone across the western regions of the WIS (Zelt, 1985; Leithold, 1993, 1994; Kowallis et al., 1989; Kowallis et al., 1995; Desmares et al., 2007; and references therein); and 5) is stratigraphically confined by a regional basal unconformity (Zelt, 1985; Eaton et al., 1990; Tucker et al., 2020). In most localities studied within Utah, the ash bed TT1 has generally been identified as consisting of one ash bed, but two distinct beds have been identified at some study areas in southwestern Utah and Pueblo (Elder, 1985; Zelt, 1985). Locally in Central Utah, historical and recent biostratigraphic frameworks indicated an upper Cenomanian temporal placement, not limited to: 1) the molluscan genera *Inoceramas*, *Euomphaloceras* and *Mytiloides submytiloides* Seitz (1934) (Zelt, 1985; Kirschbaum and Schenk, 2010, Fig. 3; Eaton et al., 1990, Table 1, pp. 42); 2) various palynomorphs (Garrison et al., 2007; and references therein; Barclay et al., 2015); and 3) trackway studies by Kirkland et al. (2016), Joyce et al. (2016) and Lockley et al. (2018). Support for these original age estimates includes age dating of the underlying Mussentuchit Member (Cifelli et al., 1997, 1999; Garrison et al., 2007; Tucker et al., 2020). In Tucker et al. (2020), a detrital zircon sample obtained from the Naturita to constrain the underlying Mussentuchit Member established via CA-TIMS analysis that the lowermost Naturita in the Wasatch Plateau is no older than 95.64 ± 0.11 Ma. Although slightly younger, the CA-TIMS-based maximum depositional age (MDA) is within reason of reported age dates of 96.06 Ma for the middle Naturita by Dyman et al. (2002), ~94–95 Ma by Barclay et al. (2015), and most recently 95.98 ± 0.12 Ma by Laurin et al. (2019).

TT4 has most recently been associated with the *Pseudaspidoceras flexuosum* biozone (Leithold and Dean, 1998, Fig. 2; Li and Schieber, 2018, Fig. 3) or the *Vascoceras birchbyi* subzone that forms part of the *Watinoceras coloradoense* biozone (Tibert et al., 2003, Fig. 2; Tibert and Leckie, 2013, Fig. 3; Jones et al., 2019, Fig. 2) in the south-central regions of Utah. Turonian-aged molluscs, such as *M. mytiloides* Mantell (1822), *M. latus* (Sowerby in Eaton et al., 1990), *M. labiatus* Schlotheim (1813 in Eaton et al., 1990) and *Morrowites* (Cobban and Hook, 1983), have been stratigraphically associated with TT5, with their more basally-oriented absence used to identify the stratigraphic placement of TT4 (Zelt,

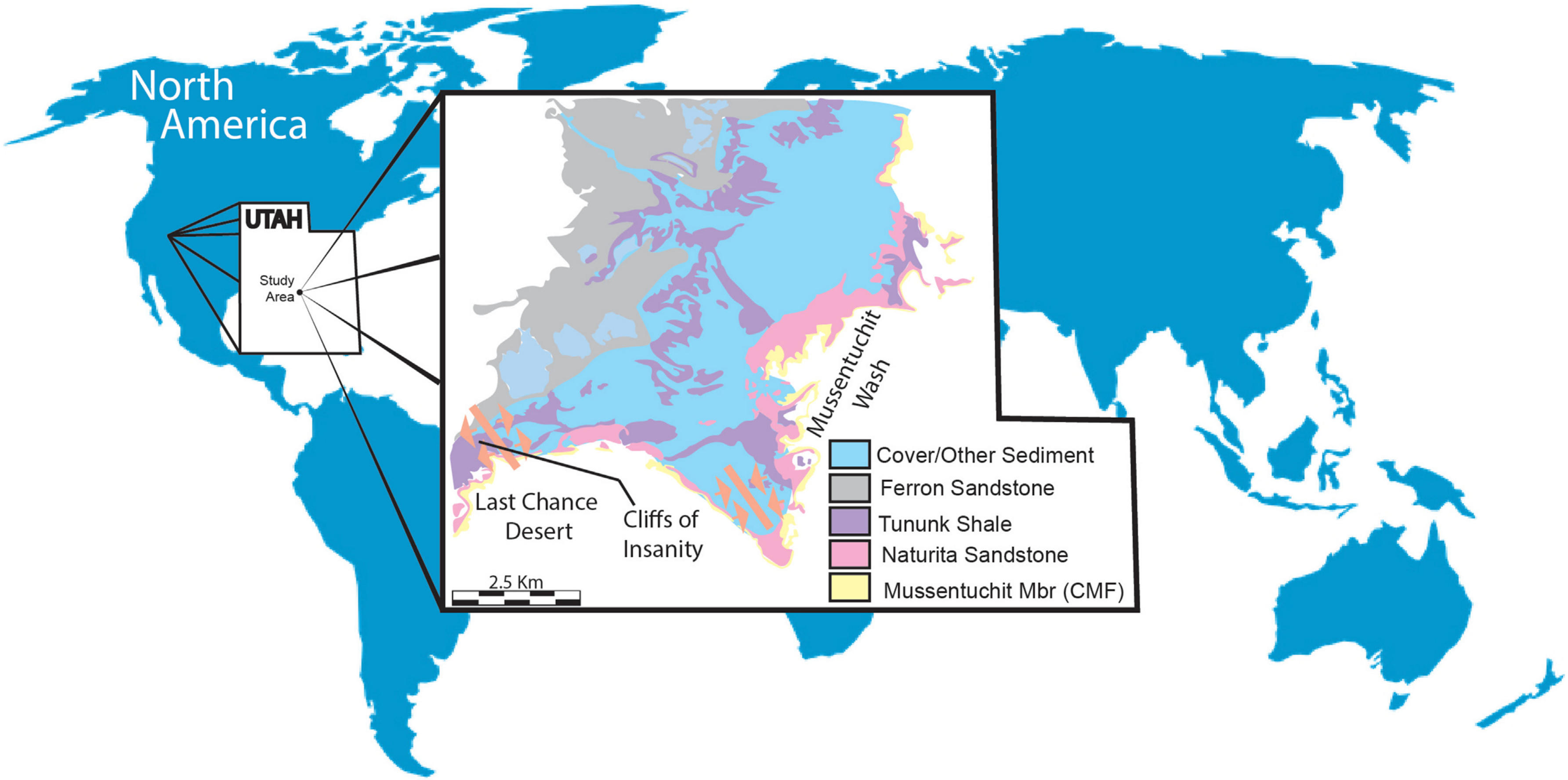

Fig. 1. Location of the surficial deposits of the Naturita Sandstone and Tununk Shale just south of the Wasatch Plateau, Central Utah, in between the northern Last Chance Desert ("Cliffs of Insanity") and the Mussentuchit Wash (Modified from the Utah Geological Survey).

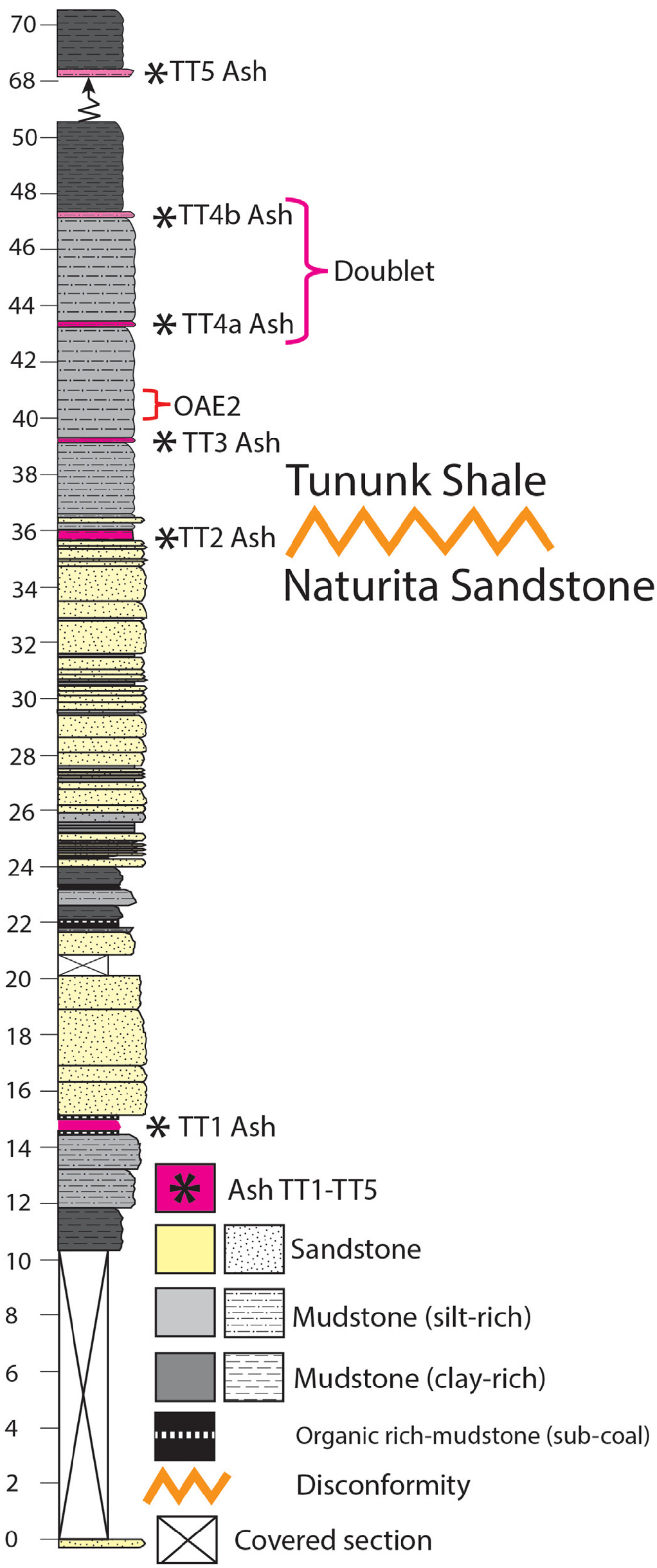

Fig. 2. General stratigraphic column of the Naturita Sandstone and the Tununk Shale, in the northern Last Chance Desert ("Cliffs of Insanity") and the Mussentuchit Wash. Relative position of the TT1 to TT5 ashes in the Naturita and Tununk locally.

1985; Eaton et al., 1990; Leithold, 1994; Li and Schieber, 2018). In the study area, the fifth ash bed is consistent in that it is further spaced apart than ashes TT2–TT4 as shown by Zelt (1985), Leithold (1994), and Li and Schieber (2018). This suggests that the sampled ash in the study area is the lower bed of the TT4 doublet. For the sake of clarity, this study has designated the term doublet as used by Ryer et al. (1980) for the TT4a and TT4b bentonite pair, with TT4b overlying the TT4a bentonite at the study locality. To the authors' current knowledge, no geochronological data regarding TT4a or TT4b in the study area is published (Fig. 3), although some geochronological data from the south-western region of Utah is available for bentonite marker bed D (Jones et al., 2021).

2.4. The Cenomanian–Turonian boundary event/Oceanic Anoxic Event (OAE2)

The Cenomanian–Turonian anoxic event (OAE2) is a well-known and extensively studied ocean anoxic event recording global carbon (and oxygen) cycle disturbances (e.g., Jenkyns, 1980; Scholle and Arthur, 1980; Pratt and Threlkeld, 1984; Tsikos et al., 2004; Keller et al., 2004; Boudinot et al., 2020; Bryant et al., 2021); carbon isotope ($\delta^{13}C$) data associated with the OAE2 make this geological event an ideal stratigraphic benchmark, locally and regionally (e.g., Joo and Sageman, 2014; Jones et al., 2019). For instance, a significant positive carbon isotopic excursion of between 4 and 6‰ has been recognized in both the Tropic Formation of the southern Kaiparowits Plateau (Utah) and the Bridge Creek Limestone Formation at the Pueblo Stratotype (Colorado; e.g., Pratt and Threlkeld, 1984; Keller et al., 2004; Sageman et al., 2006; Joo and Sageman, 2014; Jones et al., 2019, Jones et al., 2021). Isotopic data indicates three distinct phases associated with the OAE2: 1) an 'initiation' phase, including a temporally brief but distinct positive excursion which correlates with the upper *Metoicoceras mosbyense* and lower *S. gracile* biozones (Sageman et al., 2006, fig. 1; 'A' in Pratt and Threlkeld, 1984; Joo and Sageman, 2014; 'CIE phase' in Boudinot et al., 2020) and subsequent negative excursion, extending biostratigraphically over the *S. gracile* biozone ('B' in Pratt and Threlkeld, 1984; Joo and Sageman, 2014; 'Plenus phase' in Gale and Christensen, 1996; Boudinot et al., 2020); 2) a 'plateau' phase, an extensive positive excursion extending from the upper *S. gracile* biozone in the Kaiparowits Plateau and the *Neocardioceras juddii* biozone at the Pueblo stratotype to the *W. devonense* biozones at both areas ('C' in Pratt and Threlkeld, 1984; Joo and Sageman, 2014; 'plateau' in Tsikos et al., 2004; Sageman et al., 2006; Jones et al., 2019; Boudinot et al., 2020); and 3) a 'recovery' phase, where values return near a pre-event background composition either defined by the end-of-plateau commencement of depletion or an extended longer depletion to pre-event values (e.g., Sageman et al., 2006; Eldrett et al., 2015; Jones et al., 2019; Boudinot et al., 2020). Data for the Kaiparowits Plateau, Pueblo Stratotype, and associated cores (e.g., Iona-1, Portland, Angus, SH #1) show that TT1 generally falls within the 'initiation' phase, with TT2 and TT3 falling within the 'plateau' phase (Boudinot et al., 2020; Jones et al., 2021). Irrespective of the differing estimates of the termination duration of the OAE2 (e.g., end-of-plateau vs. longer; e.g., Tsikos et al., 2004; Sageman et al., 2006; Jones et al., 2019), TT4 occurs temporally within sediments that have recorded depleted or background $\delta^{13}C$ isotopic compositions (Sageman et al., 2006; Joo and Sageman, 2014; Jones et al., 2019; Boudinot et al., 2020). Comparison to the three aforementioned phases of the OAE2 can therefore improve correlations and relative chronostratigraphy between WIS localities.

3. Methods

In a previous field season, the authors collected and processed several key detrital zircon samples from the Mussentuchit Member of the Cedar Mountain Formation and the overlying basal Naturita Sandstone (Tucker et al., 2020). The 95.64 Ma age date recovered from the lowermost portion of the most basal trough-bedded

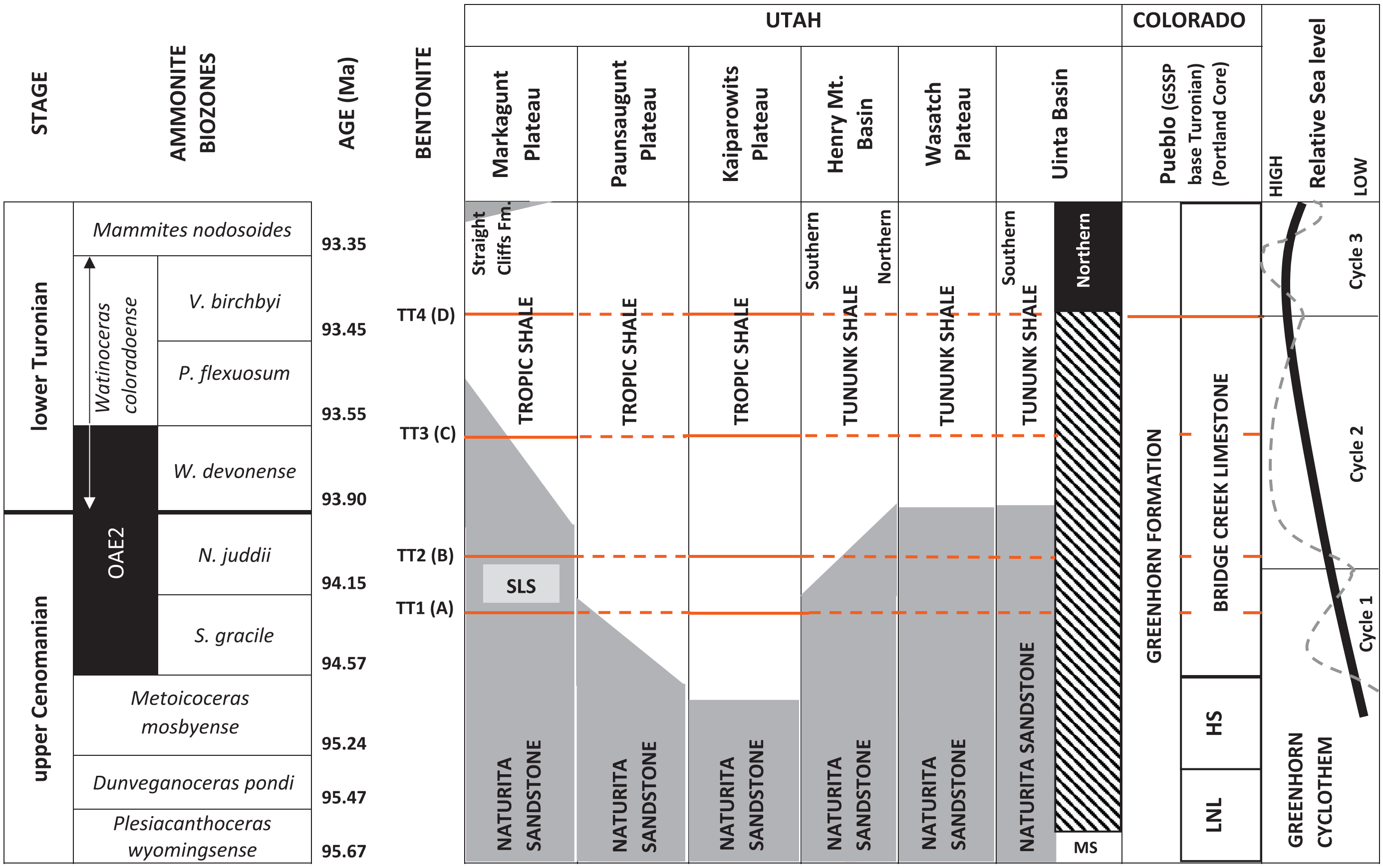

Fig. 3. A generalized summary of upper Cenomanian and lower Turonian lithostratigraphy (Zelt, 1985; Leithold, 1994; Tibert et al., 2003; Currie et al., 2012; Sprinkel et al., 2012; Tibert and Leckie, 2013; Jones et al., 2019), ammonite biostratigraphy (adapted from Kirkland, 1991; Kauffman et al., 1993; Ogg and Hinnov, 2012) and bentonite beds (A–D of Elder, 1985; TT1–TT4 of Leithold, 1994) adapted from Tibert et al. (2003) and Jones et al. (2019) from the major basins and plateaus of Utah, as well as the base Turonian global boundary stratotype section and point at Pueblo, Colorado. The ages of the biozones are taken from the 2012 Geologic Time Scale (GTS) (Ogg and Hinnov, 2012; and references therein). (1) OAE2 – Oceanic Anoxic Event; (2) Fm. – Formation; (3) SLS – Sugarledge Sandstone; (4) Mt. – Mountain; (5) GSSP – Global Boundary Stratotype Section and Point; (6) LNL – Lincoln Limestone; (7) HS – Hartland Shale; (8) MS – Mowry Shale. Orange lines indicate chronostratigraphic markers with dashed lines indicating the absence of age dates of the relevant bentonites. Gray dashed line indicates small scale approximate relative sea rise and thick black line represents approximate large scale relative sea level rise of the Greenhorn transgression adapted from Tibert et al. (2003) and Jones et al. (2019).

sandstone was thought to be a meaningful detrital zircon CA-TIMS-based MDA, and is being revised currently (Tucker et al., 2022). In the 2019 field season, ash-fall samples were discovered and collected in two locations; 1) a tonstein in the Naturita Sandstone; and 2) the lowermost bentonite of a doublet (TT4a) in the overlying Tununk Shale (Mancos Shale), in the very northern Last Chance Desert (informally known as the "Cliffs of Insanity"), south of the Wasatch Plateau (Fig. 1). All samples were collected from fresh, unweathered, and unaltered strata, typically ±1.0–1.5 m below the surface. Two gallon-sized bags of ash were collected at each site and processed according to the techniques set forth by the Central Analytical Facility at Stellenbosch University including crushing, milling, panning, Frantz magnetic separation, and density liquid separation. Thereafter, all analyses of the recovered zircon grains were analyzed by coauthor J. Crowley at Boise State University's Isotope Geology Laboratory (Boise, Idaho, USA).

3.1. CA-TIMS (U–Pb)

U–Pb dates were obtained by the CA-TIMS method from analyses composed of single zircon grains (Table 1), modified after Mattinson (2005). Zircon was selected for TIMS dating based on Cathoduluminescense (CL) images and LA-ICP-MS dates. In the two rock samples, grain separates that yielded the five youngest LA-ICP-MS dates from an initial round were analyzed in a second round. U–Pb age dates from both rounds agreed in most cases. Grains were selected for CA-TIMS from this population. For a third sample, the grains were too small to permit a second round of analysis.

Zircon was put into 3 ml Teflon PFA beakers and loaded into 300 ml Teflon PFA microcapsules. Fifteen microcapsules were placed in a large-capacity Parr vessel and the zircon partially dissolved in 120 ml of 29 M HF for 12 h at 190 °C. The zircon was returned to 3 ml Teflon PFA beakers, HF was removed, and the zircon was immersed in 3.5 M HNO_3, ultrasonically cleaned for an hour, and fluxed on a hotplate at 80 °C for an hour. The HNO_3 was removed and the zircon was rinsed twice in ultrapure H_2O before being reloaded into the 300 ml Teflon PFA microcapsules (rinsed and fluxed in 6 M HCl during sonication and washing of the zircon) and spiked with the EARTHTIME mixed ^{233}U–^{235}U–^{202}Pb–^{205}Pb tracer solution (ET2535). Zircon was dissolved in Parr vessels in 120 ml of 29 M HF with a trace of 3.5 M HNO_3 at 220 °C for 48 h, dried to fluorides, and re-dissolved in 6 M HCl at 180 °C overnight. U and Pb were separated from the zircon matrix using an HCl-based anion-exchange chromatographic procedure (Krogh, 1973), eluted together, and dried with 2 μl of 0.05 NH_3PO_4.

Pb and U were loaded on a single outgassed Re filament in 5 μl of a silica-gel/phosphoric acid mixture (Gerstenberger and Haase, 1997), and U and Pb isotopic measurements made on a GV Isoprobe-T multicollector thermal ionization mass spectrometer

Table 1
For grains recovered from the Naturita Ash, six grains were analyzed by CA-TIMS, the three youngest of which have a weighted mean of 94.616 ± 0.027 Ma (MSWD = 1.1, probability of fit = 0.35). This is the interpreted depositional age. Three grains that yield dates of 97.783 ± 0.058 to 95.128 ± 0.038 Ma are interpreted as containing inherited or detrital components (antecrysts). For grains recovered from the Tununk Shale, six grains were analyzed by CA-TIMS, the four youngest of which have a weighted mean of 94.007 ± 0.017 Ma (MSWD = 1.6, probability of fit = 0.19). This is the interpreted depositional age. Two grains that yield dates of 94.838 ± 0.033 to 94.127 ± 0.035 Ma are interpreted as containing inherited or detrital components (antecrysts). Reader should note: a) z1, z2, etc. are labels for analyses composed of single zircon grains that were annealed and chemically abraded (Mattinson, 2005) and z1a and z1b are fragments from the same grain. b) Model Th–U ratio calculated from radiogenic $^{208}Pb-^{206}Pb$ ratio and $^{207}Pb-^{235}U$ date; c) Pb* and Pbc are radiogenic and common Pb, respectively mol % 206Pb* is with respect to radiogenic and blank Pb; d) Measured ratio corrected for spike and fractionation only. Fractionation correction for single-collector Daly analyses is based on measurement of 202Pb/205Pb in the EARTHTIME ET2535 tracer solution; e) Corrected for fractionation and spike. Common Pb in zircon analyses is assigned to procedural blank with composition of $^{206}Pb-^{204}Pb = 18.04 \pm 0.61\%$; $^{207}Pb-^{204}Pb = 15.54 \pm 0.52\%$; $^{208}Pb-^{204}Pb = 37.69 \pm 0.63\%$ (1 sigma). $^{206}Pb-^{238}U$ and $^{207}Pb-^{206}Pb$ ratios corrected for initial disequilibrium in $^{230}Th-^{238}U$ using a D(Th–U) of 0.20 ± 0.05 (1 sigma); (f) Errors are 2 sigma, propagated using algorithms of Schmitz and Schoene (2007) and Crowley et al. (2007); (g) Calculations based on the decay constants of Jaffey et al. (1971). $^{206}Pb-^{238}U$ and $^{207}Pb-^{206}Pb$ dates corrected for initial disequilibrium in $^{230}Th-^{238}U$ using a D(Th–U) of 0.20 ± 0.05 (1 sigma).

								Radiogenic isotope ratios								Isotopic dates					
Sample (a)	LA-ICPMS label	$\frac{Th}{U}$ (b)	$^{206}Pb^*$ $\times 10^{-13}$ mol (c)	mol % $^{206}Pb^*$ (c)	$\frac{Pb^*}{Pb_c}$ (c)	Pb_c (pg) (c)	$\frac{^{206}Pb}{^{204}Pb}$ (d)	$\frac{^{208}Pb}{^{206}Pb}$ (e)	$\frac{^{207}Pb}{^{206}Pb}$ (e)	% Err (f)	$\frac{^{207}Pb}{^{235}U}$ (e)	% Err (f)	$\frac{^{206}Pb}{^{238}U}$ (e)	% Err (f)	Corr. Coef.	$\frac{^{207}Pb}{^{206}Pb}$ (g)	± (f)	$\frac{^{207}Pb}{^{235}U}$ (g)	± (f)	$\frac{^{206}Pb}{^{238}U}$ (g)	± (f)
Naturita Ash																					
z6		0.517	1.0512	98.27%	17.1	1.54	1040	0.165	0.048070	0.378	0.101256	0.402	0.015284	0.059	0.467	101.63	8.95	97.93	0.38	97.783	0.058
z4	53	0.590	0.1528	99.01%	30.9	0.13	1830	0.189	0.048259	0.365	0.099379	0.391	0.014942	0.059	0.498	110.92	8.62	96.20	0.36	95.610	0.056
z1	50	0.577	1.0756	99.82%	166.0	0.16	9789	0.185	0.048011	0.075	0.098365	0.093	0.014866	0.041	0.615	98.72	1.78	95.27	0.08	95.128	0.038
z3	54	0.548	0.2580	99.40%	50.6	0.13	3018	0.175	0.048006	0.220	0.097848	0.237	0.014789	0.047	0.463	98.51	5.20	94.79	0.21	94.640	0.044
z2	44	0.454	0.0.3719	99.59%	72.6	0.13	4438	0.145	0.047961	0.178	0.097714	0.194	0.014783	0.042	0.485	96.27	4.20	94.66	0.18	94.600	0.040
z7		0.494	0.4207	97.65%	12.5	0.84	769	0.158	0.048131	0.525	0.098060	0.556	0.014783	0.077	0.465	104.67	12.40	94.98	0.50	94.598	0.072
TFA #1 & #2																					
z1 – TFA #2	355	0.398	1.0081	99.82%	158.0	0.15	9781	0.127	0.047995	0.061	0.098033	0.079	0.014821	0.035	0.696	97.98	1.44	94.96	0.07	94.838	0.033
z3 – TFA #2	363	0.416	0.9249	99.76%	121.4	0.19	7477	0.133	0.0.047986	0.083	0.097272	0.097	0.014709	0.037	0.569	97.49	1.95	94.26	0.09	94.127	0.035
z1 – TFA #1	339	0.387	1.3518	99.84%	179.0	0.18	11,110	0.124	0.047950	0.054	0.097088	0.071	0.014692	0.031	0.713	95.73	1.28	94.08	0.06	94.020	0.029
z2 – TFA #2	361	0.377	1.0361	99.84%	176.9	0.14	11,012	0.120	0.048006	0.067	0.097195	0.084	0.014691	0.037	0.634	98.52	1.58	94.18	0.08	94.013	0.035
z3 – TFA #2	342	0.433	1.1943	99.77%	126.3	0.23	7744	0.139	0.047977	0.068	0.097133	0.083	0.014690	0.035	0.624	97.09	1.60	94.13	0.07	94.010	0.033
z2 – TFA #2	340	0.369	1.4065	99.87%	224.4	0.15	13,993	0.118	0.048012	0.059	0.097158	0.082	0.014683	0.044	0.714	98.79	1.40	94.15	0.07	93.967	0.041

equipped with an ion-counting Daly detector. Pb isotopes were measured by peak-jumping all isotopes on the Daly detector for 160 cycles and corrected for mass fractionation using the known $^{202}Pb-^{205}Pb$ ratio of the ET2535 tracer solution. Transitory isobaric interferences due to high-molecular-weight organics, particularly on ^{204}Pb and ^{207}Pb, disappeared within approximately 30 cycles, while ionization efficiency averaged 10^4 cps/pg of each Pb isotope. Linearity (to $\geq 1.4 \times 10^6$ cps) and the associated deadtime correction of the Daly detector were determined by analysis of NBS982. Uranium was analyzed as UO_2^+ ions in static Faraday mode on 10^{12} Ω resistors for 300 cycles and corrected for isobaric interference of $^{233}U^{18}O^{16}O$ on $^{235}U^{16}O^{16}O$ with an $^{18}O-^{16}O$ of 0.00206. Ionization efficiency averaged 20 mV/ng of each U isotope. U mass fractionation was corrected using the known $^{233}U-^{235}U$ ratio of the ET2535 tracer solution.

U–Pb dates and uncertainties were calculated using the algorithms of Schmitz and Schoene (2007), calibration of ET2535 tracer solution (Condon et al., 2015) of $^{235}U-^{205}Pb = 100.233$, $^{233}U-^{235}U = 0.99506$, $^{205}Pb-^{204}Pb = 8474$, and $^{202}Pb-^{205}Pb = 0.99924$, U decay constants recommended by Jaffey et al. (1971), and $^{238}U-^{235}U$ of 137.818 (Hiess et al., 2012). The $^{206}Pb-^{238}U$ ratios and dates were corrected for initial ^{230}Th disequilibrium using $D_{Th\text{-}U} = 0.2 \pm 0.1$ (2 s) and the algorithms of Crowley et al. (2007), resulting in an increase in the $^{206}Pb-^{238}U$ dates of ~0.09 Ma. All common Pb in analyses was attributed to laboratory blank and subtracted based on the measured laboratory Pb isotopic composition and associated uncertainty. U blanks are estimated at 0.013 pg.

Weighted mean $^{206}Pb-^{238}U$ and $^{207}Pb-^{206}Pb$ dates are calculated from equivalent dates (probability of fit > 0.05) using Isoplot 3.0 (Ludwig, 2003). Errors on weighted mean $^{206}Pb-^{238}U$ dates are given as ±x/y/z, where x is the internal error based on analytical uncertainties only, including counting statistics, subtraction of tracer solution, and blank and initial common Pb subtraction, y includes the tracer calibration uncertainty propagated in quadrature, and z includes the ^{238}U decay constant uncertainty propagated in quadrature. Internal errors should be considered when comparing our dates with $^{206}Pb-^{238}U$ dates from other laboratories that used the same tracer solution or a tracer solution that was cross-calibrated using EARTHTIME gravimetric standards. Errors including the uncertainty in the tracer calibration should be considered when comparing our dates with those derived from other geochronological methods using the U–Pb decay scheme (e.g., laser ablation ICP-MS). Errors including uncertainties in the tracer calibration and ^{238}U decay constant (Jaffey et al., 1971) should be considered when comparing our dates with those derived from other decay schemes (e.g., $^{40}Ar-^{39}Ar$, $^{187}Re-^{187}Os$). Errors are at 2 s. Young ages (via LA-ICP-MS) have specifically undergone secondary ablation with results within 1% of the initial age. Young ages via CA-TIMS have also been secondarily assessed (archived fragments) with results also well-within 2σ and 1% of the initial age reported.

3.2. LA-ICP-MS (U–Pb)

For interpretation of provenance and synchronicity between volcanism and sedimentation, this study utilized LA-ICP-MS-based results. Zircon grains were separated from rocks using standard techniques, annealed at 900 °C for 60 h in a muffle furnace, and randomly selected grains were mounted in epoxy and polished until their centers were exposed. CL images were obtained with a JEOL JSM-300 scanning electron microscope and Gatan MiniCL. Zircon was analyzed by laser ablation inductively coupled plasma mass spectrometry (LA-ICP-MS) using a ThermoElectron X-Series II quadrupole ICP-MS and New Wave Research UP-213 Nd: YAG UV (213 nm) laser ablation system. In-house analytical protocols, standard materials, and data reduction software were used for the acquisition and calibration of U–Pb dates and a suite of high field strength elements (HFSE) and rare earth elements (REE). Zircon was ablated with a laser spot of 25 μm wide using fluence and pulse rates of 5 J/cm^2 and 5 Hz, respectively, during a 45-s analysis (15-s gas blank, 30-s ablation) that excavated a pit ~25 μm deep. Ablated material was carried by a 1.2 L/min He gas stream to the nebulizer flow of the plasma. Quadrupole dwell times were 5 ms for Si and Zr, 200 ms for ^{49}Ti and ^{207}Pb, 80 ms for ^{206}Pb, 40 ms for ^{202}Hg, ^{204}Pb, ^{208}Pb, ^{232}Th, and ^{238}U and 10 ms for all other HFSE and REE; total sweep duration is 950 ms. Background count rates for each analyte were obtained prior to each spot analysis and subtracted from the raw count rate for each analyte. For concentration calculations, background-subtracted count rates for each analyte were internally normalized to ^{29}Si and calibrated with respect to NIST SRM-610 and -612 glasses as the primary standards. Ablation pits that appear to have intersected glass or mineral inclusions were identified based on Ti and P signal excursions, and associated sweeps were discarded. U–Pb dates from these analyses are considered valid if the U–Pb ratios appear to have been unaffected by the inclusions. Signals at mass 204 were normally indistinguishable from zero following subtraction of mercury backgrounds measured during the gas blank (<1000 cps ^{202}Hg), and thus dates are reported without common Pb correction. Rare analyses that appear contaminated by common Pb were rejected based on mass 204 greater than baseline. Temperature was calculated from the Ti-in-zircon thermometer (Watson et al., 2006). Because there are no constraints on the activity of TiO_2, an average value in crustal rocks of 0.8 was used.

Data were collected in four experiments in July 2020. For U–Pb and $^{207}Pb-^{206}Pb$ dates, instrumental fractionation of the background-subtracted ratios was corrected and dates were calibrated with respect to interspersed measurements of zircon standards and reference materials. The primary standard Plešovice zircon (Sláma et al., 2008) was used to monitor time-dependent instrumental fractionation based on two analyses for every 10 analyses of unknown zircon. A secondary correction to the $^{206}Pb-^{238}U$ dates was made based on results from the zircon standards Seiland (530 Ma, unpublished data, Boise State University) and Zirconia (327 Ma, unpublished data, Boise State University), which were treated as unknowns and measured once for every 10 analyses of unknown zircon. These results showed a linear age bias of several percent that is related to the ^{206}Pb count rate. The secondary correction is thought to mitigate matrix-dependent variations due to contrasting compositions and ablation characteristics between the Plešovice zircon and other standards (and unknowns).

Radiogenic isotope ratio and age error propagation for all analyses include uncertainty contributions from counting statistics and background subtraction. The standard calibration uncertainty for U–Pb is the local standard deviation of the polynomial fit to the fractionation factor of Plešovice versus time and for $^{207}Pb-^{206}Pb$ is the standard error of the mean of the fractionation factor of Plešovice. These uncertainties are 0.6–1.0% (2 s) for $^{206}P-^{238}U$ and 0.2–0.5% (2 s) for $^{207}Pb-^{206}Pb$. Age interpretations are based on $^{206}Pb-^{238}U$ dates. Errors on the dates are given at 2 s.

3.3. Carbon isotopes ($\delta^{13}C_{org}$)

Carbon isotope samples were collected from cleaned or trenched outcrop at regular intervals (~0.2 m) throughout the Naturita Sandstone and Tununk Shale. Bulk sediment samples were collected from primarily fine-grained or carbon-rich units, and subsamples for $\delta^{13}C_{org}$ analyses were prepared by first removing any surficial modern organic material via repeated ultrasonication of samples in methanol. All samples were then dried and reacted with a dilute solution of HCl (7–10%) at 40 °C to remove all carbonate material and rinsed with deionized water until cleaned/neutralised. Samples were dried and ground/homogenized before being loaded into tin capsules for isotopic analysis using a Costech elemental analyzer attached to a Thermo Delta V+ isotope ratio mass spectrometer at North Carolina State University's Paleo^3 Laboratory. Organic carbon isotope ($\delta^{13}C_{org}$) measurements are reported in units per mil (‰) relative to the Vienna Pee Dee Belemnite (VPDB) and used IAEA sucrose (−10.45‰) and caffeine (−27.77‰) standards for calibration. Analytical uncertainty is maintained at <0.1‰, and replicate analyses of organic carbon samples had a mean standard error of 0.3‰.

4. Results

Bulk samples of the Naturita and Tununk ash-fall deposits contain minor amounts of rounding or surficial fractures/cracks on individual grains with the majority presenting pristine euhedral well-faceted zircons (Fig. 4). Zircon grains commonly exhibit simple bimodal to growth zoning, with many preserving distinct cores and an occasional inclusion (Fig. 4). Within this study, we also utilized an MDA for comparison based on recent U–Pb detrital zircon geochronology from the basal-most trough bedded sandstone in the Naturita (Tucker et al., 2020). All Depositional Ages (DA's) and Maximum Depositional Ages (MDA's) are based on CA-TIMS results (Online supplementary Fig. 1; Tucker et al., 2020).

4.1. CA-TIMS DA and MDA

Based on the prior study by Tucker et al. (2020), the basal sediments of the Naturita are no later than ± 95.64 ± 0.11 Ma; yet, multiple studies have long-suspected these sediments to be reworked from the downcutting of the upper Mussentuchit Member of the Cedar Mountain Formation (Eaton et al., 1990; Garrison et al., 2007; Tucker et al., 2023, In Review). Therefore, this study utilized the 95.64 ± 0.11 Ma to assess the possibility of reworking in the overlying upper Naturita Sandstone and Tununk Shale respectively. From the Naturita Ash (TT1), six grains were analyzed via CA-TIMS, with the three youngest grains having a weighted mean of 94.616 ± 0.027 Ma (MSWD = 1.1, probability of fit = 0.35) (Table 2). The remaining three grains yield dates between 95.128 ± 0.038 and 97.783 ± 0.058 Ma and are interpreted as antecrysts (containing inherited or detrital components). With a distinct lack of sedimentological reworking of this syndepositional ash, we interpret this sample to contain a mixture of autocrysts and antecrysts (Fig. 5). Therefore, the most youthful grains around 94.616 ± 0.027 Ma, are interpreted as autocrysts, are the nearest to syndeposition and indicate a meaningful DA (Fig. 5).

Similar to the Naturita ash, six grains were selected from the Tununk Ash (TT4) and analyzed via CA-TIMS (Fig. 5). Again, a minor spread of dates was present, representing a mixture of autocrysts and antecrysts. The grains yielding the four youngest dates are interpreted as autocrysts, and nearest to syndepositional; thus, a meaningful DA. The weighted mean of these four dates is 94.007 ± 0.017 Ma (MSWD = 1.6, probability of fit = 0.19) (Fig. 5; Table 2). The remaining grains yielded dates of 94.838 ± 0.033 and 94.127 ± 0.035 Ma are herein interpreted as antecrysts (Fig. 5). These two particular antecrysts yield dates similar to the DA of the underlying Naturita Sandstone. Therefore, based on the DA's mentioned above, this study supports the conclusions of previous studies which chronostratigraphical places the sediments of the Naturita and the lower Tununk near to the C–T Boundary (Ogg and Hinnov, 2012; Cohen et al., 2013b, v2020/03).

4.2. LA-ICP-MS-based provenance

Due to the well-documented tectonic history and a well-formed backbone of prior work (Willis, 1999; Dickinson and Gehrels, 2003; DeCelles, 2004; Dickinson and Gehrels, 2009a,b; Laskowski et al., 2013; and references therein), we can draw meaningful linkages to likely source terranes. Mesozoic-aged grains constitute a vast majority of all recovered ages from all three bulk samples, and of this, an overwhelming majority fall between the Cenomanian and Turonian respectively (±89.8–100.5 Ma). As a whole, the zircon age spectra(s) presented in the three samples, along with a probability density plot strongly reflect a collisional, foreland basin (as identified by Cawood et al., 2012; pp. 876, fig. 1D) (Online supplementary Fig. 2). As discussed in Tucker et al. (2020), a vast majority of grain ages in the Naturita Sandstone are Mesozoic; however, minor populations of Precambrian or Paleozoic grains are present. All ashfall grain ages recovered from the Naturita and Tununk are between the Cenomanian and Turonian. Pre-Cambrian or Paleozoic grain ages recovered from the basal Naturita are interpreted to be reworked from a variety of terranes. A vast majority of youthful grain ages from all three samples fall within Phase C (pulse of volcanism from 105 to 80 Ma) of arc volcanism identified by DeCelles and Graham (2015) (Online supplementary Fig. 2). Therefore, much of the regional correlations to potential source terranes rely on well-documented Laurentian-margin orogenic systems along the southern Cordilleran margin (DeCelles, 2004; Gehrels and Pecha, 2014; Tucker et al., 2020). This study also holds to the fact that these younger grains are likely from a variety of volcanic inliers, within the expansive western lying Cordilleran Arc.

For ash-fall samples, air currents likely mobilized ash-rich clouds from the westerly-lying arc into the easterly basins and, if minor mobilization via hydraulic systems occurs with any of these samples, we would expect regional drainage oriented to the northeast and boreal waters flowing southward (Dickinson and Gehrels, 2008; Suarez et al., 2012; Lowery et al., 2018; and references therein). Therefore, westerly to southwesterly lying source terranes within North American Cordillera are the more-likely contributors of most youthful grain ages (Dickinson and Gehrels, 2008; Lawton et al., 2010; Hunt et al., 2011; Laskowski et al., 2013; Szwarc et al., 2015; Brown et al., 2018; Pecha et al., 2018). The longer-lived source terranes (130 ± 90 Ma) include the Northern Sierra Nevada, Central Sierra Nevada Batholith (Western Coast Plutonic Complex), and Peninsular Ranges Batholith. Recognized, more localized tectonic events that could have also contributed zircons between 118 Ma and 92 Ma include the Black Rock Arc Terrane, Sierra Crest Magmatic Event, Sahwave/Nightingale Range, Santa Rosa Range, Crowsnest, and the Bloody Run Hills (Brown et al., 2018). Additionally, air circulation models for the Cenomanian are interpreted to have flowed northwest to southeast-east across the northern and central Laramidia. Although less likely, circulating winds could carry zircon-rich ash-fall to the central portion of the Western Interior Seaway (Central Utah) from central-north to northern source terranes (Hay and Floegel, 2012; Lowery et al., 2018; Tucker et al., 2020). These include the Owyhee Mountains, Atlanta Lobe of the Idaho Batholith and Eastern Coast Plutonic Complex (Gaschnig et al., 2009; Finzel, 2017; Sauer et al., 2017; Brown et al., 2018; Quinn et al., 2018).

4.3. LA-ICP-MS-based K–S test

We utilized the Kolmogorov-Smirnov test (K–S test) to evaluate the likelihood that the age profiles of zircons at sites are genetically similar ($p > 0.05$; i.e., not statistically different) or dissimilar ($p < 0.05$). Statistically dissimilar samples suggest that the samples

Fig. 4. Cathodoluminescence images of zircon. Grains selected for CA-TIMS are shown with analysis labels, as are locations of LA-ICP-MS spots with analysis labels.

originated from different (possibly multiple) source terranes across the North American Craton; whereas, statistically similar samples argue for near-syndepositional grain ages and multi-grain populations that are derived from the same source terrane (DeGraaff-Surplus et al., 2003; Barbeau et al., 2009; Guynn and Gehrels, 2010). Although this method and its accuracy remain tenuous, when results from the K–S test are coupled with other results within this study, there is a strong argument for the appropriateness of the K–S test on this dataset. When all three samples are compared, detrital zircons recovered from the basal Naturita Sandstone (Tucker et al., 2020) share 0.00 genetic likelihood with either ash samples. Yet, the ash-fall recovered from the Naturita and Tununk do share 0.22 genetic likelihood. This weak genetic similarity may reflect the difference in progressively younger samples progressing up-section. Based on these results, we identify the source difference between the detrital zircons of the basal-most Naturita Sandstone and that of the recovered ash-fall from the Naturita and Tununk.

Table 2
Weighted mean calculations, MSWD = mean square of weighted deviation. pof = probability of fit.

Sample (a)	Weighted mean calculations		
Naturita ash			
z6		206Pb/238U ± random (+tracer) [+decay constant]	MSWD = 1.1
z4		**94,616 ± 0.027** (0.054) [0.115]	pof = 0.35
z1			n = 3
z3	x		
z2	x		
z7	x		
TFA #1 & #2			
z1 − TFA #2		206Pb/238U ± random (+tracer) [+decay constant]	MSWD = 1.6
z3 − TFA #2		**94,007 ± 0.017** (0.050) [0.112]	pof = 0.19
z1 − TFA #1	x		n = 4
z2 − TFA #2	x		
z3 − TFA #2	x		
z2 − TFA #2	x		

Bold text signifies the depositional age (DA) based on the MSWD assessment.

4.4. CA-TIMS-based coeval/non-coeval volcanics

Coupling of the results of the K–S test and MDA's allows us to determine whether there was contemporaneous sedimentation and volcanic activity (Rossignol et al., 2019; Tucker et al., 2020). It should be noted that the basal Naturita MDA and the ash-fall DAs interpreted from CA-TIMS display a distinct younging trend (Fig. 6). The presented CA-TIMS DA's confirm the synchronicity between sedimentation and volcanic activity. Based on CA-TIMS, Δt1–Δt3 (Δt-change in time) would indicate a very short emplacement period, roughly Δt = 1.76 Ma between this interval of Naturita and Tununk deposition (Fig. 6).

4.5. Carbon isotopes

Carbon isotope ($\delta^{13}C_{org}$) values range from −10.2‰ to −25.6‰ (VPDB) throughout the section, with an average value of −23.5‰ (SD = 2.7‰). The data shows a distinct trend with stratigraphic height, where all enriched values (>−24‰) are restricted to the section between 38 and 47 m and all highly enriched values (>−20‰) are restricted to the section between 40 and 45 m (Fig. 6). Reprocessed and reanalyzed samples (see Section 5) were slightly depleted relative to initial analyses (Fig. 6), but confirm the strong carbon isotope excursion and overall enriched values observed from 40 to 45 m stratigraphic height in the lower Tununk Shale (between TT3 and TT4b ashes).

5. Discussion

We identify the TT1 locally as a syndepositional ash-fall within the Naturita, with a DA of 94.616 Ma. We can, therefore, confidently correlate the lower Naturita Sandstone and the TT1 to the following ash beds as cited in previous literature: 1) T1 in the Kaiparowits Plateau (Grand Staircase-Escalante National Monument, Southern Utah) and Henry Mountain Basin (Zelt, 1985; Li and Schieber, 2018); 2) PBC-5 of the Bridge Creek Limestone Member of the Greenhorn Limestone Formation (Pueblo, Colorado-event-isochronous designations, which correlates to between 20,000 and 100,000 years per event interval) (Elder, 1985; Elder and Kirkland, 1985; Kowallis et al., 1989; Kowallis et al., 1995); 3) beds 69–71 of Graneros Shale and Greenhorn Limestone Near Pueblo, Colorado (Cobban and Scott, 1972; Elder and Kirkland, 1985; Kennedy et al., 2005; Sageman et al., 2006) and 4) bentonite “A” exposed near Pueblo, Colorado (Fig. 7) (Elder, 1985, 1988; Meyers et al., 2012; Laurin et al., 2019). Similarly, we identify the TT4a locally as a syndepositional ash-fall within the lower Tununk Shale, with a DA of 94.010 Ma. Therefore, our study confidently correlates the lower Tununk Shale and the TT4a to the following ash beds as cited in literature pertaining to the WIS: 1) T4 in the Kaiparowits Plateau (Grand Staircase-Escalante National Monument, Southern Utah) and Henry Basin (Zelt, 1985; Li and Schieber, 2018); 2) PBC-20 of the Bridge Creek Limestone Member of the Greenhorn Limestone Formation (Pueblo, Colorado) (Elder, 1985; Elder and Kirkland, 1985; Kowallis et al., 1989; Kowallis et al., 1995); 3) beds 91–97 of Graneros Shale and Greenhorn Limestone near Pueblo, Colorado (Cobban and Scott, 1972; Elder and Kirkland, 1985; Kennedy et al., 2005; Sageman et al., 2006) and 4) bentonite “D” exposed near Pueblo, Colorado (Fig. 7) (Elder, 1985; Elder and Kirkland, 1985; Elder, 1988; Meyers et al., 2012; Laurin et al., 2019). These DA's suggest a fairly rapid emplacement of sediment and volcanilithics (ash-fall) into this particular depocenter, likely reflecting regional tectonism. This observation is supported by the interpretation of the local detrital MDA of 95.64 Ma from the basal Naturita obtained via CA-TIMS by Tucker et al. (2020) as reworked from the uppermost Mussentuchit Member (uppermost Cedar Mountain Formation) rather than syndepositional (Garrison et al., 2007; Tucker et al., 2023, In Review).

The locally-based TT1 and TT4a age estimations are within meaningful uncertainty of other regionally-based U–Pb zircon radiometric age dating by Barclay et al. (2015) and Laurin et al. (2019); however, both studies noted a mixture of autocrysts and antecrysts, similar to this study (Fig. 7). By utilizing both LA-ICP-MS and CA-TIMS our study is confident in identifying both the most youthful zircons (autocrysts) and providing a rigorous syndepositional DA for the TT1 and TT4a locally. Regional-based support for the above-mentioned late Cenomanian placement for the TT1 include the most laterally persistent Bridge Creek Limestone markers LS2 and LS3 (Elder, 1985; Elder and Kirkland, 1985) and individual unit designations 69–71 of the Bridge Creek Limestone (Cobban and Scott, 1972; Zelt, 1985; Kennedy et al., 2005; Sageman et al., 2006) and extensive biostratigraphic correlations (Kennedy et al., 2005; Cobban et al., 2006). For instance, a Cenomanian temporal placement for the TT1 co-occurs with key biostratigraphic taxa including the mollusc *I. pictus* and the occurrence (prior to the diversification), of the genus *Mytiloides* (especially within Utah) (Kennedy et al., 2005; Ogg and Hinnov, 2012; Meyers et al., 2012; Jones et al., 2021), which has also been observed to occur in close association with TT1 in the Wasatch Plateau area (Zelt, 1985). However, regionally our results do not correlate with the $^{40}Ar–^{39}Ar$ (sanidine)-based age placement of the TT1 as dated by Kowallis et al. (1995) from the Tropic Shale of southern Utah and the equivalent Bridge Creek Limestone in the four corners as well as the 93.68 ± 0.50 Ma date as given by Cobban et al. (2006). This particular difference likely reflects both, the mineral systems used to obtain the age date and the lack of recalibration of the standard Fish Canyon Tuff as discussed in Kuiper et al. (2008).

Conversely, age dates recovered from the northern and northeastern regions of the Uinta Basin yield significantly different results. Specifically, for the TT1, the intra-basinal correlation of the Naturita Sandstone remains cryptic across the northern, eastern and southern regions of the Uinta Basin (Molenaar and Cobban, 1991; Currie et al., 2012; Sprinkel et al., 2012). Currently, the use of three hiatus-based divisions of the Naturita Sandstone are recognized via lithological features and the presence or absence of key marine and terrestrial palynomorphs (Currie, 2002; Currie et al., 2012; Sprinkel et al., 2012). This is complemented by Sprinkel et al. (2012), who obtained an ash-fall U–Pb zircon-based age date for the lowermost division in the eastern region of the

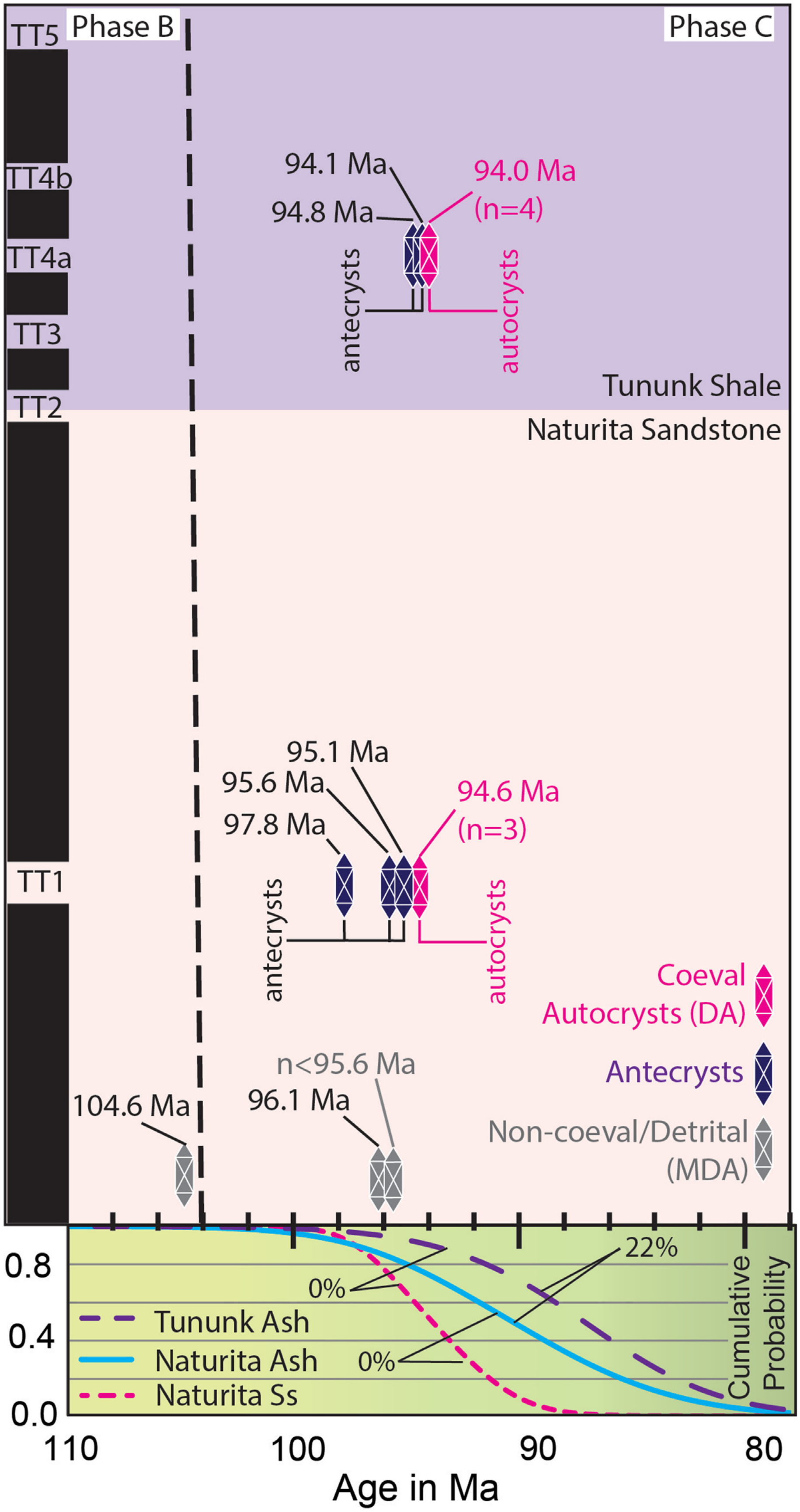

Fig. 5. Temporal relationship of grain ages recovered from the TT1 and TT4a, along with detrital grain ages recovered from the basal Naturita Sandstone from Tucker et al. (2020). Antecrysts presented in gray and autocrysts presented in pink along with the number of grains within that most youthful population. (1) Ss – Sandstone.

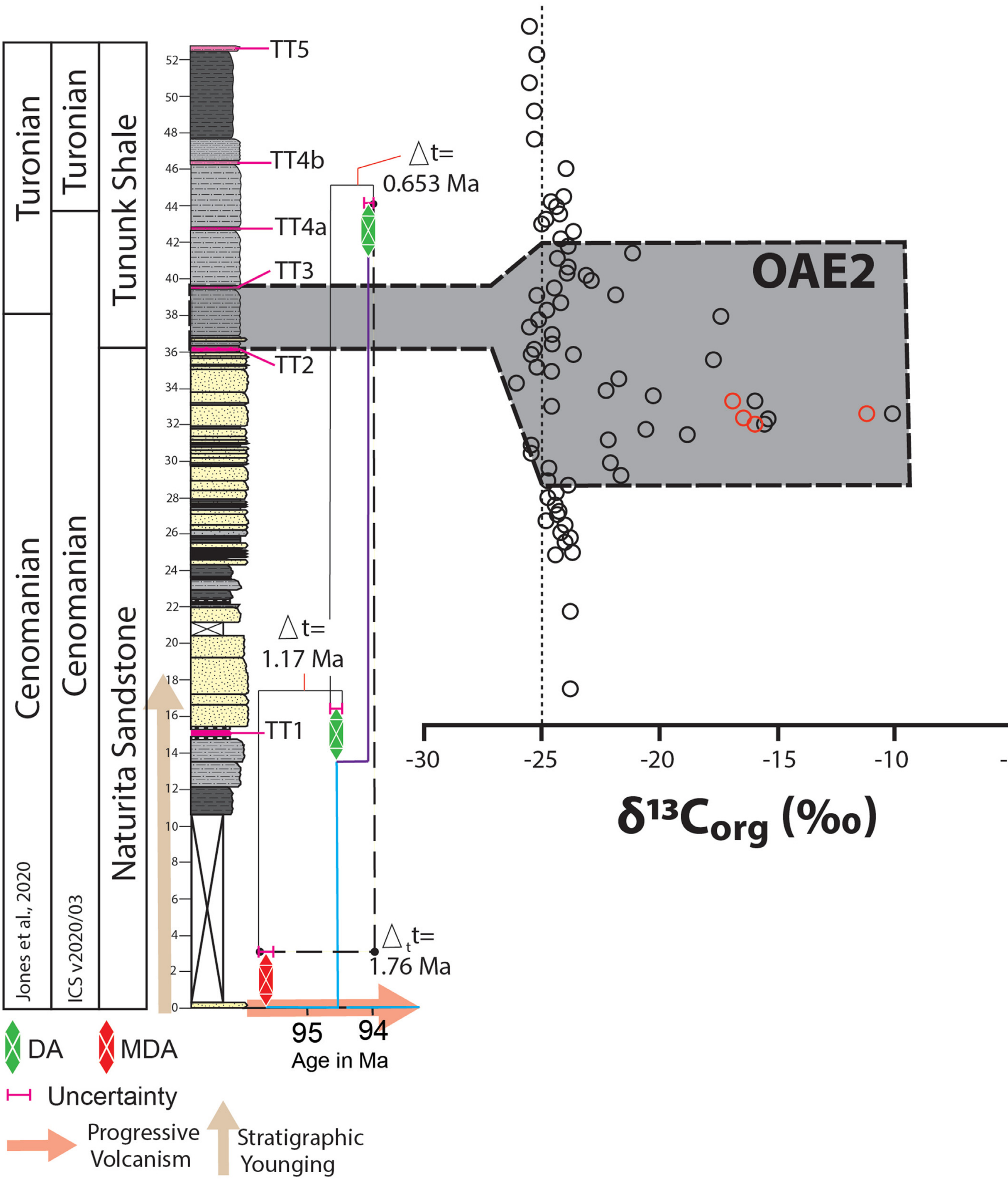

Fig. 6. Displaying the synchronous nature of volcanic activity and sedimentation input into the local depocenter. The relationship of relative stratigraphic age and the progressively youthful zircon populations indicate a strong contemporaneity (see Rossignol et al., 2019; fig. 14). Figure displays the most recently published regional Cenomanian–Turonian contact (Jones et al., 2021) and the internationally assigned Cenomanian–Turonian contact (Cohen et al., 2013b, v2020/03). Carbon isotope ($\delta^{13}C_{org}$) stratigraphy of the upper Naturita and Tununk Formations. Circles indicate individual samples, where uncertainty/standard error is smaller than the symbol. Red data indicate reprocessed/reanalyzed samples from the same horizons. Shaded box highlights interval correlated to the Cenomanian–Turonian anoxic event (OAE2) based on the observed carbon isotopic excursions, with the lighter shaded portion corresponding to the 'recovery' phase (c.f., Jones et al., 2019).

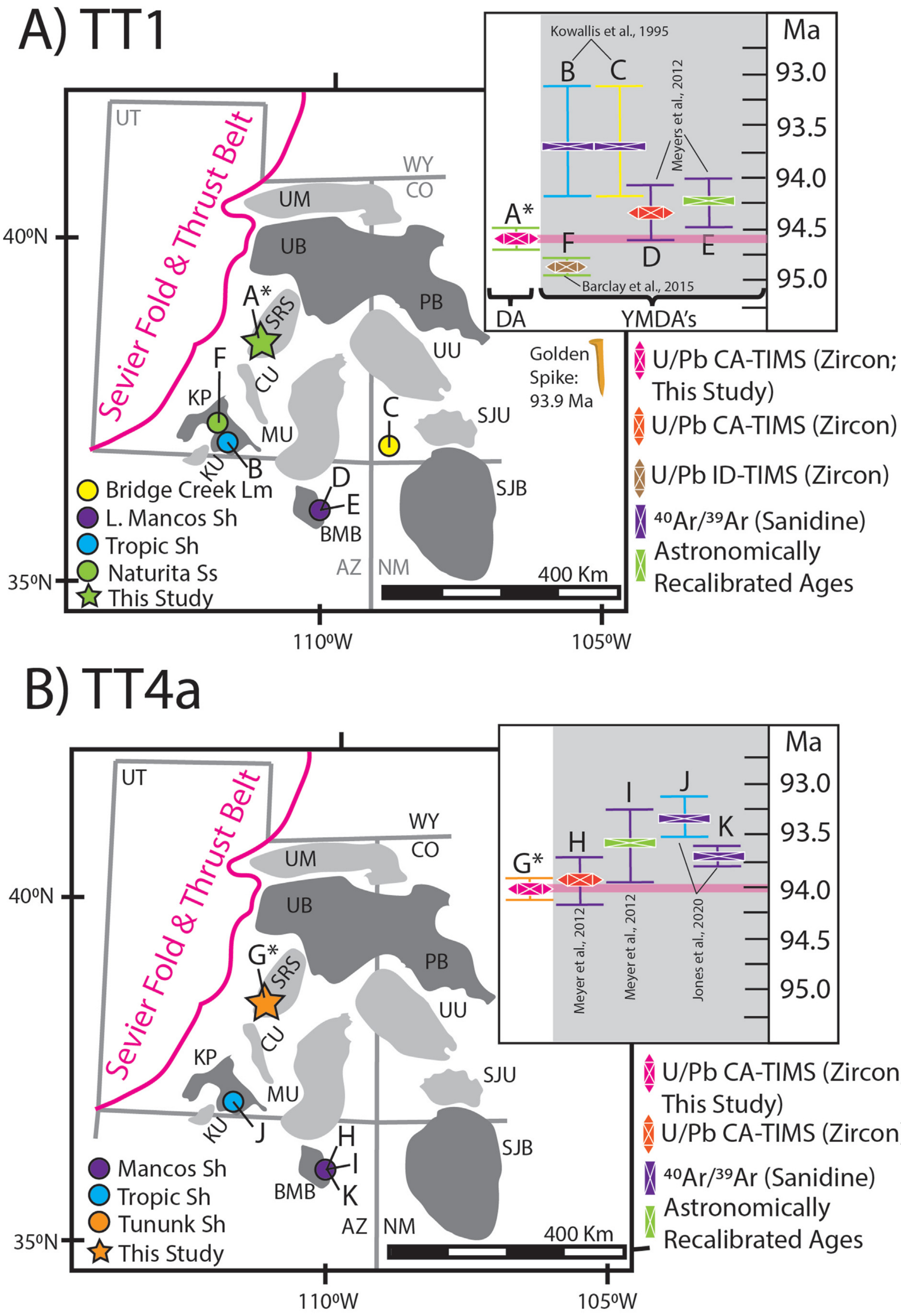

A) TT1
UT
WY
CO
Sevier Fold & Thrust Belt
UM
UB
PB
UU
SJU
SJB
SRS
CU
KP
MU
KU
BMB
AZ
NM
A*
B
C
D
E
F
40⁰N
35⁰N
110⁰W
105⁰W
400 Km
Bridge Creek Lm
L. Mancos Sh
Tropic Sh
Naturita Ss
This Study
Golden Spike: 93.9 Ma
Kowallis et al., 1995
Meyers et al., 2012
Barclay et al., 2015
Ma
93.0
93.5
94.0
94.5
95.0
DA
YMDA's
U/Pb CA-TIMS (Zircon; This Study)
U/Pb CA-TIMS (Zircon)
U/Pb ID-TIMS (Zircon)
40Ar/39Ar (Sanidine)
Astronomically Recalibrated Ages
B) TT4a
UT
WY
CO
Sevier Fold & Thrust Belt
UM
UB
PB
UU
SJU
SJB
SRS
CU
KP
MU
KU
BMB
AZ
NM
G*
H
I
J
K
40⁰N
35⁰N
110⁰W
105⁰W
400 Km
Mancos Sh
Tropic Sh
Tununk Sh
This Study
Meyer et al., 2012
Meyer et al., 2012
Jones et al., 2020
Ma
93.0
93.5
94.0
94.5
95.0
U/Pb CA-TIMS (Zircon; This Study)
U/Pb CA-TIMS (Zircon)
40Ar/39Ar (Sanidine)
Astronomically Recalibrated Ages

Uinta Basin to be 101.4 ± 0.4 Ma. Therefore, the two-overlying hiatus-based divisions are suspected to be also late Albian in age (Currie, 2002; Currie et al., 2012; Sprinkel et al., 2012). Further temporal constraint is extrapolated from the overlying Arrow Creek bentonite (southwestern Wyoming) at the base of the Mowry Shale via $^{40}Ar-^{39}Ar$ (sanidine) with an age date of 98.5 ± 0.5 Ma (Obradovich, 1993) and the overlying Clay Spur bentonite (southwestern Wyoming) via $^{40}Ar-^{39}Ar$ (sanidine) with an age date of 97.2 ± 0.7 and 98.17 ± 0.11 Ma (Obradovich, 1993; Singer et al., 2020). Based on these calibrated units, the Naturita and overlying units in the Uinta Basin were emplaced earlier than those of the Last Chance Desert (Molenaar and Wilson, 1990; Molenaar and Cobban, 1991; Sprinkel et al., 2012). However, palynological data and ammonite fossils suggest that the uppermost part of the second division of the Naturita Sandstone in the southern Uinta Basin is of Cenomanian age; thus, more contemporaneous with other regions of Utah (Molenaar and Cobban, 1991; and references therein). Although this may indicate a prolonged, diachronous emplacement of the Naturita Sandstone progressing southward, resolving this is beyond the scope of this manuscript.

$^{40}Ar-^{39}Ar$ (sanidine; Jones et al., 2021) and U–Pb age dates (Meyers et al., 2012; Stangroom, 2012, unpublished data) obtained for TT4 (Fig. 7) as well as the most laterally persistent Bridge Creek Limestone markers LS10 and LS11 (Elder, 1985; Elder and Kirkland, 1985) and individual unit designations 90–97 of the Bridge Creek Limestone (Cobban and Scott, 1972; Zelt, 1985; Kennedy et al., 2005; Sageman et al., 2006) support an early Turonian emplacement of the TT4 (a and b) ash layer. Biostratigraphical correlations, including the occurrence of several species belonging to the genera *Mytiloides* and/or *Watinoceras*, as well as the noticeable absence of the genus *Inoceramus* (Zelt, 1985; Eaton et al., 1990; Leithold, 1994; Kennedy et al., 2005), concur with these results. Historically, age date resolution of TT4 has been problematic; the absence of suitable minerals for $^{40}Ar-^{39}Ar$ age dating (Kowallis et al., 1995), the presence of detrital material (AZLP-08-05, Lohali Point, Arizona; Meyers et al., 2012) and anomalous data obtained from Nipple Creek in southern Utah by Jones et al. (2021; NC-D; Nipple Creek outcrop, Utah) have prevented anchoring and correlation of dates for TT4 (a and b) across the WIS. The older age date obtained in this study does not correlate with the re-calibrated dates obtained from samples of Obradovich (1993) and Meyers et al. (2012) from Lohali Point, Arizona (Jones et al., 2021). However, as TT4b is the stratigraphically thicker bentonite of the doublet (Zelt, 1985; Eaton et al., 1990), it is, therefore, more likely to be the most laterally continuous. Therefore, it is plausible that the aforementioned authors sampled and dated this bentonite, not TT4a, and this may account for the older age date obtained in this study. Regardless, as the data in this study has been obtained using the aforementioned blended analysis, we report the first high precision U–Pb age date associated with TT4 for the central region of Utah.

Within this newly constructed temporal range extending from TT1 (94.616 Ma) to TT4 (94.010 Ma), the lower transgressive portion of the Greenhorn Cyclothem is constrained locally. The rapid emplacement of both these ashes provides valuable information regarding the regional incursion of the Greenhorn Seaway. Prior to the deposition of TT1 in the southern regions of Utah, initial transgression began in the northern to northeastern regions, as evidenced by the correlatively older Naturita strata (late Albian) and Mowry Shale (early to middle Cenomanian) of the Uinta Basin (Molenaar and Wilson, 1990; Molenaar and Cobban, 1991; Currie et al., 2012; Sprinkel et al., 2012). Moving geographically from southwestern to south-central Utah, the TT1 was emplaced within the marginal-marine and shallow marine facies of the Naturita Sandstone (Markagunt Plateau) (Laurin et al., 2019), and the offshore mudstone and shale strata of the Tropic Shale and Tununk Shale of the south-central Kaiparowits Plateau and the Henry Mountain basin. This is indicative of the progressive flooding of this area by the southward migration of the Greenhorn Sea and marks the position of the late Cenomanian highstand shoreline in the Markagunt Plateau. TT1 in the Naturita Sandstone of the Wasatch Plateau is present in the first thick coal interval, suggesting a local initial rapid-base level rise. These coastal plain deposits are overlaid by transgressive ravinement as a result of subsequent flooding, followed by offshore deposits and shallower shoreface deposits (Garrison et al., 2007). In the measured section herein (Fig. 2), on top of these shallow marine deposits is an ash deposit (TT2), which is followed within a few decimeters by *P. newberryi* lag indicating transgressive ravinement and flooding of the Wasatch Plateau during the *N. juddii* biozone. TT3 is present above this, with the next ash TT4 (a and b), occurring locally, and in the Henry Mountain Basin, within the Tununk Shale, as well as within the Tropic Shale of the Kaiparowits Plateau. The Tununk Shale and Tropic Shale are regionally correlative to the Bridge Creek Limestone of the four corners regions and the southern central regions surrounding Pueblo, Colorado. The regional age date of the TT4 occurs close to the transition between the second and third cycles which records local sea level cyclicity at the base of the peak 4th-order cycle of the Greenhorn transgression (Leithold, 1994; Jones et al., 2019).

Carbon isotope ($\delta^{13}C_{org}$) values define the OAE2, as indicated by a positive δ13C excursion just before the TT3 through just below the TT4b ash in the lower Tununk Shale (~39–47 m), with peak or 'plateau' values falling between the TT3 and TT4a ashes (~40–42 m) followed by a 'recovery' with progressive depletion back to baseline by TT4b (Fig. 6). Baseline pre- and post-event carbon isotope values are stable around ~−25‰ with carbon isotope excursion values generally 3–7‰ more enriched, though some samples appear as much as 15‰ enriched, which may be a result of depositional conditions (i.e. peat bogs with macrophytes (Boutton, 1991; Santos et al., 2017)) (Fig. 6). While all values in this outcrop section are slightly enriched relative to many contemporaneous core records, the magnitude and duration/placement of what can be interpreted as the plateau phase of the OAE2 (Boudinot et al., 2020 and references therein) compares favorably to other records of this latter OAE2 stage from the localized Greenhorn transgression (e.g., Jones et al., 2018; Boudinot and Seplúveda, 2020) and elsewhere in the Western Interior Basin (e.g., Keller et al., 2004; Joo and Sageman, 2014; Forkner et al., 2021). The slightly enriched baseline of our record and enhancement of the δ13C excursion in this section may be due to the marginal-marine nature of the locality, a characteristic observed in other similar records (e.g., Laurin et al., 2019). The marginal marine character of this locality (e.g., Figs. 1, 2), associated with the later incursion of the Greenhorn Seaway, may also explain why the geochemical expression of the OAE2 here is mostly restricted to between TT3 and TT4, whereas at other more distal/deeper-water localities (e.g., Keller et al., 2004; Joo and Sageman, 2014) this chronostratigraphically significant event appears more extended (initiating between TT1 and TT2, plateauing around TT3, and resolving by TT4). This could suggest that anoxia in the WIS initiated in the central basin and shoaled/spread through the OAE2 event (c.f., Laurin et al., 2019), eventually encompassing marginal localities with anoxic/euxinic conditions during the 'plateau' phase

Fig. 7. Regional comparison of temporal placement of the TT1 and TT4(a) compared with this study's results (light gray). (1) UB – Uinta Basin; (2) PB – Piceance Creek Basin; (3) SJB – San Juan Basin; (dark gray); (4) KP – Kaiparowits Plateau; (5) KU – Kaibab Uplift; (6) CU – Circle Uplift; (7) MU – Monument Upwarp; (8) SRS – San Rafael Swell; (9) SJU – San Juan Uplift; (10) UU – Uncompahgre Uplift; (11) UM – Uinta Mountains; (12) BMB – Black Mesa Basin.

of the event and resolving roughly contemporaneously everywhere (e.g., Fig. 6; Joo and Sageman, 2014; Boudinot et al., 2020).

Samples which appeared heavily or excessively enriched during the plateau phase as interpreted from our data (>7‰), were initially suspected to represent contamination by inorganic carbon (e.g., calcite); however, these samples were reprocessed to ensure complete decarbonation (via repeated concentrated HCl) and subsequent analyses produced similarly enriched $\delta^{13}C_{org}$ values (Fig. 6). This suggests that the extreme enrichment is a feature of the carbon record in these local environments; evaluations from restricted anoxic/euxinic basins have suggested that localized methanogenesis and sulfate reduction in these environments leads to buildups of recalcitrant carbon which can account for extreme enrichment of sediment $\delta^{13}C_{org}$ compositions on relatively short timescales (e.g., Londry and Des Marais, 2003; Conrad et al., 2009). Therefore, these values in the lower Tununk (particularly from ~40 to 45 m; Fig. 6) may be associated with highly anoxic/euxinic conditions in these restricted or marginal Greenhorn deposits, providing additional evidence for OAE2 impacts in this interval. Overall, the observed positive values recorded at our study area correlates to the plateau phase of the Cenomanian–Turonian anoxic event/OAE2 recorded throughout the WIB constrained here to occurring between TT1 (94.616 Ma) and TT4 (94.010 Ma), with the ‘recovery’ phase and associated C–T boundary likely closer to the end of this interval (TT3–TT4; Fig. 6).

Therefore, paired carbon isotopes and U–Pb radiometric dating of the zircon-rich ash fall provides a framework to constrain the temporal occurrence of major Late Cretaceous geological events such as the OAE2 and the C–T boundary across the WIS. Although the CIE phase of the OAE2 in the WIS is associated temporally with the deposition of the *S. gracile* biozone (Laurin and Sageman, 2007; Jones et al., 2019; Laurin et al., 2019) and ranges through to the *W. coloradoense* biozone (Jones et al., 2021), it is most likely to have occurred locally during the *N. juddii* and subsequent early Turonian biozones due to the later transgression of the Greenhorn Seaway. According to our data, the temporal occurrence of the plateau phase within the Wasatch Plateau is constrained to 94.616 Ma and 94.007 Ma, which is well within the range of uncertainties produced by other studies (Sageman et al., 2006; Turgeon and Creaser, 2008; Meyers et al., 2012; van Helmond et al., 2015; van Helmond et al., 2016; Eldrett et al., 2017; O'Connor et al., 2020; Jones et al., 2021). Ash falls TT1 (94.616 Ma)–TT4 (94.010 Ma) span the C–T boundary (constrained to within a 600k period), the boundary itself occurring between TT2 and TT3, which has been regionally dated at Nipple Creek near Big Water in Southern Utah at 94.082 ± 0.057 Ma (TT2) and 94.011 ± 0.060 (TT3) (Obradovich, 1993; Meyers et al., 2012; Jones et al., 2021). Although TT2 and TT3 are at present undated locally, this is the subject of current research and will be discussed in a later manuscript. At present, the International Commission on Stratigraphy (Cohen et al., 2013b, v2020/03) has globally standardized the C–T boundary as occurring at approximately 93.90 Ma. Although it is not the purpose of this study to resolve the geochronological placing of the C–T boundary, our results bolster support that the sediments deposited between TT1 and TT4 occurred during the Cenomanian–Turonian transition and are locally and regionally diachronous. These results draw attention to the fact that further research into refining the C–T boundary date should continue to be a priority (Gradstein and Ogg, 2004; Cohen et al., 2013a, v2019/05; Cohen et al., 2013b, v2020/03).

6. Conclusion

The following conclusions can be drawn from the geochronological study of ash-fall marker beds TT1 and TT4 from the Wasatch Plateau of the central Utah region.

1. This study assessed six zircons from the Naturita Ash via CA-TIMS that resulted in identifying three antecrysts and three autocrysts. Based on the weighted mean calculation, the Naturita Ash (TT1) in the Last Chance Desert of the Wasatch Plateau yielded an age of 94.616 ± 0.027 Ma. This supports a previous emplacement age for the Naturita Sandstone in this area of 95.6 Ma. However, this study finds it more likely that the 95.6 Ma grain ages recovered from the basal Naturita trough-bedded sandstone are equivalent to the underlying Mussentuchit Member of the Cedar Mountain Formation.
2. This study assessed six zircons from the Tununk Ash via CA-TIMS that resulted in identifying four autocrysts and two antecrysts. Based on the weighted mean calculation, the Tununk Ash (TT4a) in the Last Chance Desert of the Wasatch Plateau yielded an age of 94.007 ± 0.017 Ma. TT4 bentonite yielded an age date older than most of the geochronological data reported in the literature. However, a significant portion of geochronological data provided by past studies has been marred by the absence of datable minerals, presence of detrital zircons or anomalous dates obtained (Kowallis et al., 1995; Meyers et al., 2012; Jones et al., 2021).
3. Comparison of the stratigraphic placement of the TT1 and TT4 across Utah indicates that the transgression of the Greenhorn Sea occurred in the northeastern regions prior to the south, central or western areas. The emplacement of TT1 within the Naturita Sandstone, a sediment recording environmental changes in what is interpreted as mostly a terrestrial environment, indicates that the western region of the San Rafael Swell may have formed one of the last transgressional surfaces during the late Cenomanian–early Turonian.
4. The age dates obtained may assist in further constraining the Cenomanian–Turonian Boundary to between 94.616 and 94.007 Ma. The locally obtained age range for the C–T boundary is marginally older than those obtained by previous studies, as well as the internationally recognized age of 93.90 ± 0.15 Ma as proposed by ICS. Accurately dating this stage boundary is particularly important geologically and biostratigraphically, as the C–T boundary is a geochronological standard against which other geological and boundary events are dated.
5. A contemporaneous relationship between sedimentation and volcanism between 95 and 94 Ma has been established for the study area. Several cycles of volcanism and sedimentation related to the transgression of the Greenhorn Sea are recorded within the deposits, indicating that several pulses of volcanic activity, associated with uplift in the western regions of the WIS.
6. Carbon isotope chemostratigraphy highlights a distinct (~3–7‰) carbon isotope excursion in the lower Tununk Shale (TT3 through TT4), identified here as the plateau phase of the Cenomanian–Turonian OAE2 in the WIS.

Data availability

Data will be made available on request.

Acknowledgments

We thank staff, students, and volunteers of the 2015–2019 expeditions to the Mussentuchit Member of the CMF; M. Leschin, S. Foss, G. McDonald, R. Anderson, R. Hunt-Foster, J. Kirkland, M. Hayden, J. Krishna, R. Irmis, staff of the Price Field Office, the Bureau of Land Management Utah State Office, Natural History Museum of Utah, and Utah Geological Survey for permitting and expedition support. We thank K. McKinney of the USGS for his help with locating some documents regarding biozone(s). We would also like to thank the anonymous reviewers for their detailed and helpful comments that have significantly improved this manuscript. Financial support was provided by Stellenbosch University's Department of Earth Sciences, North Carolina Museum of Natural Sciences, and the Canyonlands Natural History Association. This material is based upon work supported by the National Science Foundation under Grant No FRES 1925973 (to LEZ and EGH). Any opinions, findings, and conclusions or recommendations expressed in this material are those of the author(s) and do not necessarily reflect the views of the National Science Foundation.

References

Arthur, M.A., Schlanger, S.O., Jenkyns, H.C., 1987. The Cenomanian-Turonian oceanic anoxic event II, paleoceanographic controls on organic matter production and preservation. In: Brooks, J., Fleet, A. (Eds.), Marine Petroleum Source Rocks, Geological Society Special Publications, vol. 24, pp. 399–418. London.

Barbeau Jr., D.L., Gombosi, D.J., Zahid, K.M., Bizimis, M., Swanson-Hysell, N., Valencia, V., Gehrels, G.E., 2009. U-Pb zircon constraints on the age provenance of the Rocas Verdes basin fill, Tierra del Fuego, Argentina. Geochemistry, Geophysics, Geosystems 10, 1–11.

Barclay, R.S., Rioux, M., Meyer, L.B., Bowring, S.A., Johnson, K.R., Miller, I.M., 2015. High precision U-Pb zircon geochronology for Cenomanian Dakota Formation floras in Utah. Cretaceous Research 52, 213–237.

Boudinot, F.G., Sepúlveda, J., 2020. Marine organic carbon burial increased forest fire frequency during Oceanic Anoxic Event 2. Nature Geoscience 13, 693–698.

Boudinot, F.G., Dildar, N., Leckie, R.M., Parker, A., Jones, M.M., Sageman, B.B., Bralower, T.J., Sepúlveda, J., 2020. Neritic ecosystem response to Oceanic Anoxic Event 2 in the Cretaceous Western Interior Seaway, USA. Palaeogeography, Palaeoclimatology, Palaeoecology 546, 109673. https://doi.org/10.1016/j.palaeo.2020.109673.

Boutton, T.W., 1991. Stable carbon isotope ratios of natural materials: II. Atmospheric, terrestrial, marine, and freshwater environments. In: Coleman, D.C., Fry, B. (Eds.), Carbon Isotope Techniques. Academic Press, San Diego, CA, U.S.A, pp. 173–185.

Brown, K.L., Hart, W.K., Stuck, R.J., 2018. Temporal and geochemical signatures in granitoids of northwestern Nevada: Evidence for the continuity of the Mesozoic magmatic arc through the western Great Basin. Lithosphere 10, 327–350.

Bryant, R., Leckie, R.M., Bralower, T.J., Jones, M.M., Sageman, B.B., 2021. Microfossil and geochemical records reveal high-productivity paleoenvironments in the Cretaceous Western Interior Seaway during Oceanic Anoxic Event 2. Palaeogeography, Palaeoclimatology, Palaeoecology 584, 110679. https://doi.org/10.1016/j.palaeo.2021.110679.

Caldwell, W.G.E., Diner, R., Eicher, D.L., Fowler, S.P., North, B.R., Stelck, C.R., von Holdt Wilhelm, L., 1993. Foraminiferal biostratigraphy of cretaceous marine cyclothems. In: Caldwell, W.G.E., Kauffman, E.G. (Eds.), Evolution of the Western Interior Basin, Geological Association of Canada Special Paper, vol. 39, pp. 477–520.

Carpenter, K., 2014. Where the sea meets the land-the unresolved Dakota problem in Utah, vol. 43. Utah Geological Association Publication, pp. 357–372.

Cawood, P.A., Hawkesworth, C.J., Dhuime, B., 2012. Detrital zircon record and tectonic setting. Geology 40, 875–878.

Cifelli, R.L., Kirkland, J.I., Weil, A., Deino, A.L., Kowallis, B.J., 1997. High-precision $^{40}Ar/^{39}Ar$ geochronology and the advent of North America's Late Cretaceous terrestrial fauna. Proceedings of the National Academy of Sciences 94, 11163–11167.

Cifelli, R.L., Nydam, R.L., Gardner, J.D., Weil, A., Eaton, J.G., Kirkland, J.I., Madsen, S.K., Gillette, D.D., 1999. Medial Cretaceous vertebrates from the Cedar Mountain Formation, Emery County, Utah: the Mussentuchit local fauna. In: Gillette, D.D. (Ed.), Vertebrate Fossils of Utah. Utah Geological Survey, Salt Lake City, pp. 219–242.

Cobban, W.A., Hook, S.C., 1983. Mid Cretaceous (Turonian) ammonite fauna from Fenee Lake area, west-central New Mexico, vol. 37. Memoirs of the Institute of Mining and Technology, New Mexico, pp. 1–50.

Cobban, W.A., Reeside Jr., J.B., 1952. Frontier Formation, Wyoming and adjacent areas. AAPG Bulletin 36 (10), 1913–1961.

Cobban, W.A., Scott, G.R., 1972. Stratigraphy and ammonite fauna of the Graneros Shale and Greenhorn Limestone near Pueblo, Colorado. In: United States Geological Survey Professional Paper, vol. 645.

Cobban, W.A., Walaszczyk, I., Obradovich, J.D., McKinney, K.C., 2006. A USGS Zonal Table for the Upper Cretaceous Middle Cenomanian-Maastrichtian of the Western Interior of the United States Based on Ammonites, Inoceramids, and Radiometric Ages. United States Geological Survey Open-File Report 1250, p. 46.

Cohen, K.M., Finney, S.C., Gibbard, P.L., Fan, J.X., 2013a. The ICS international chronostratigraphic chart. Episodes 36, 199–204 (v2019/05).

Cohen, K.M., Finney, S.C., Gibbard, P.L., Fan, J.X., 2013b. The ICS international chronostratigraphic chart. Episodes 36, 199–204 (updated, v2020/03).

Condon, D.J., Schoene, B., McLean, N.M., Bowring, S.A., Parrish, R.R., 2015. Metrology and traceability of U–Pb isotope dilution geochronology (EARTHTIME Tracer Calibration Part I). Geochimica et Cosmochimica Acta 164, 464–480.

Conrad, R., Claus, P., Casper, P., 2009. Characterization of stable isotope fractionation during methane production in the sediment of a eutrophic lake, Lake Dagow, Germany. Limnology & Oceanography 54, 457–471.

Crowley, J.L., Schoene, B., Bowring, S.A., 2007. U-Pb dating of zircon in the Bishop Tuff at the millennial scale. Geology 35, 1123–1126.

Currie, B.S., 1997. Sequence stratigraphy of nonmarine Jurassic–Cretaceous rocks, central Cordilleran foreland-basin system. The Geological Society of America Bulletin 109, 1206–1222.

Currie, B.S., 2002. Structural configuration of the Early Cretaceous Cordilleran foreland-basin system and Sevier thrust belt, Utah and Colorado. The Journal of Geology 110, 697–718.

Currie, B.S., McPherson, M.L., Hokanson, W., Pierson, J.S., Homan, M.B., Pyden, T., Schellenbach, W., Purcell, R., Nicklaus, D., 2012. Reservoir Characterization of the Lower Cretaceous Cedar Mountain and Dakota Formations, Northern Uinta Basin, Utah. Open-file report 597 Utah Geological Survey. Department of Natural Resources, Utah, p. 34.

D'Emic, M.D., Foreman, B.Z., Jud, N.A., Britt, B.B., Schmitz, M., Crowley, J.L., 2019. Chronostratigraphic revision of the Cloverly Formation (Lower Cretaceous, Western Interior, USA). Bulletin – Peabody Museum of Natural History 60, 3–40.

DeCelles, P.G., 2004. Late Jurassic to Eocene evolution of the Cordilleran thrust belt and foreland basin system, western USA. American Journal of Science 304, 105–168.

DeCelles, P.G., Graham, S.A., 2015. Cyclical processes in the North American Cordilleran orogenic system. Geology 43, 499–502.

DeGraaff-Surpless, K., Mahoney, J.B., Wooden, J.L., McWilliams, M.O., 2003. Lithofacies control in detrital zircon provenance studies: Insights from the Cretaceous Methow basin, southern Canadian Cordillera. The Geological Society of America Bulletin 115, 899–915.

Desmares, D., Grosheny, D., Beaudoin, B., Gardin, S., Gauthier-Lafaye, F., 2007. High resolution stratigraphic record constrained by volcanic ash beds at the Cenomanian–Turonian boundary in the Western Interior Basin, USA. Cretaceous Research 28, 561–582.

Deville, J., 1989. Coup d'oeil sur les inocérames. Mineraux et Fossiles: le Guide du Collectionneur 163, 9–14.

Dickinson, W.R., Gehrels, G.E., 2003. U–Pb ages of detrital zircons from Permian and Jurassic eolian sandstones of the Colorado Plateau, USA: Paleogeographic implications. Sedimentary Geology 163, 29–66.

Dickinson, W.R., Gehrels, G.E., 2008. Sediment delivery to the Cordilleran foreland basin: Insights from U–Pb ages of detrital zircons in Upper Jurassic and Cretaceous strata of the Colorado Plateau. American Journal of Science 308, 1041–1082.

Dickinson, W.R., Gehrels, G.E., 2009a. U–Pb ages of detrital zircons in Jurassic eolian and associated sandstones of the Colorado Plateau: Evidence for transcontinental dispersal and intraregional recycling of sediment. The Geological Society of America Bulletin 12, 408–433.

Dickinson, W.R., Gehrels, G.E., 2009b. Use of U–Pb ages of detrital zircons to infer maximum depositional ages of strata: a test against a Colorado Plateau Mesozoic database. Earth and Planetary Science Letters 288, 115–125.

Dodsworth, P., Eldrett, J.S., 2019. A dinoflagellate cyst zonation of the Cenomanian and Turonian (Upper Cretaceous) in the Western Interior, United States. Palynology 43, 701–723.

Dyman, T.S., Cobban, W.A., Davis, L.E., Eves, R.L., Pollock, G.L., Obradovich, J.D., Titus, A.L., Takahashi, K.I., Hester, T.C., Cantu, D., 2002. Upper Cretaceous Marine and Brackish Water Strata at Grand Staircase-Escalante National Monument. Geological Society of America Field Trip Road Log, Utah, p. 28.

Eaton, J.G., Kirkland, J.I., Kauffman, E.G., 1990. Evidence and dating of mid-Cretaceous tectonic activity in the San Rafael Swell, Emery County, Utah. Mountain Geologist 27, 39–45.

Eaton, J.G., Kirkland, J.I., Hutchison, J.H., Denton, R., O'Neill, R.C., Parrish, J.M., 1997. Nonmarine extinction across the Cenomanian-Turonian boundary, southwestern Utah, with a comparison to the Cretaceous-Tertiary extinction event. The Geological Society of America Bulletin 109, 560–567.

Eaton, J.G., Laurin, J., Kirkland, J.I., Tibert, N.E., Leckie, R.M., Sageman, B.B., Goldstrand, P.M., Moore, D.W., Straub, A.W., Cobban, W.A., Dalebout, J.D., 2001. Cretaceous and Early Tertiary geology of Cedar and Parowan Canyons, western Markagunt Plateau, Utah. In: Erskine, M.C., Faulds, J.E., Bartley, J.M., Rowley, P.D. (Eds.), The Geologic Transition, High Plateaus to Great Basin—A Symposium and Field Guide (The Mackin Volume), Utah Geological Association Publication 30 and American Association of Petroleum Geologists, Pacific Section Publication GB, vol. 78, pp. 337–363.

Eicher, D.L., Worstell, P., 1970. Cenomanian and Turonian Foraminifera from the Great Plains, United States. Micropaleontology, pp. 269–324.

Eicher, D.L., Diner, R., 1985. Foraminifera as indicators of watermass in the Cretaceous Greenhorn Sea, Western Interior. In: Pratt, L., Kauffman, E.G., Zelt, F.B. (Eds.), Finegrained Deposits and Biofacies of the Cretaceous Western Interior Seaway: Evidence of Cyclic Depositional Processes, Society of Economic Mineralogists and Paleontologists Field Trip No. 4, pp. 122–134.

Elder, W.P., 1985. Biotic patterns across the Cenomanian-Turonian extinction boundary near Pueblo, Colorado. In: Pratt, L.M., Kauffman, E.G., Zelt, F.B. (Eds.), Fine-grained Deposits and Biofacies of the Cretaceous Western Interior Seaway: Evidence of Cyclic Sedimentary Processes, Society of Economic Mineralogists and Paleontologists Field Trip Guidebook, vol. 4, pp. 157–169.

Elder, W.P., 1987. The paleoecology of the Cenomanian-Turonian (Cretaceous) stage boundary extinctions at Black Mesa, Arizona. PALAIOS 2, 24–40.

Elder, W.P., 1988. Geometry of Upper Cretaceous bentonite beds: Implications about volcanic source areas and paleowind patterns, western interior, United States. Geology 16 (9), 835–838.
Elder, W.P., 1989. Molluscan extinction patterns across the Cenomanian-Turonian stage boundary in the Western Interior of the United States. Paleobiology 15, 299–320.
Elder, W.P., 1991. Molluscan paleoecology and sedimentation patterns of the Cenomanian- Turonian extinction interval in the southern Colorado Plateau region. In: Nations, J.D., Eaton, J.G. (Eds.), Stratigraphy, Depositional Environments, and Sedimentary Tectonics of the Western Margin, Cretaceous Western Interior Seaway, Geological Society of America Special Paper, vol. 260, pp. 113–138.
Elder, W.P., Kirkland, J.I., 1985. Stratigraphy and depositional environments of the Bridge Creek Limestone Member of the Greenhorn Limestone at Rock Canyon Anticline near Pueblo, Colorado. In: Pratt, L.M., Kauffman, E.G., Zelt, F.B. (Eds.), Fine-grained Deposits and Biofacies of the Cretaceous Western Interior Seaway: Evidence of Cyclic Sedimentary Processes, Society of Economic Mineralogists and Paleontologists Field Trip Guidebook, vol. 4, pp. 157–169.
Elderbak, K., Leckie, R.M., 2016. Paleocirculation and foraminiferal assemblages of the Cenomanian–Turonian Bridge Creek Limestone bedding couplets: Productivity vs. dilution during OAE2. Cretaceous Research 60, 52–77.
Eldrett, J.S., Minisini, D., Bergman, S.C., 2014. Decoupling of the carbon cycle during Ocean Anoxic Event 2. Geology 42, 567–570.
Eldrett, J.S., Ma, C., Bergman, S.C., Lutz, B., Gregory, F.J., Dodsworth, P., Phipps, M., Ramezani, J., 2015. An astronomically calibrated stratigraphy of the Cenomanian, Turonian and earliest Coniacian from the Cretaceous Western Interior Seaway, USA: Implications for global chronostratigraphy. Cretaceous Research 56, 316–344.
Eldrett, J.S., Dodsworth, P., Bergman, S.C., Wright, M., Minisini, D., 2017. Water-mass evolution in the Cretaceous Western Interior Seaway of North America and equatorial Atlantic. Climate of the Past 13, 855–878.
Finzel, E.S., 2017. Detrital Zircon microtectures and U–Pb geochronology of Upper Jurassic to Paleocene strata in the distal North American Cordillera foreland basin. Tectonics 36, 1295–1316.
Forkner, R.M., Dahl, J., Fildani, A., Barbanti, S.M., Yurchenko, I.A., Moldowan, J.M., 2021. Anatomy of an extinction revealed by molecular fossils spanning OAE2. Scientific Reports 11, 13621. https://doi.org/10.1038/s41598-021-92817-5.
Gale, A.S., Christensen, W.K., 1996. Occurrence of the 5 belemnite *Actinocamax plenus* in the Cenomanian of SE France and its significance. Bulletin of the Geological Society of Denmark 43, 68–77.
Gardner, M.H., 1995. Tectonic and eustatic controls on the stratal architecture of mid-Cretaceous stratigraphic sequences, central western interior foreland basin of North America. In: Dorobek, S.L., Ross, G.M. (Eds.), Stratigraphic Evolution of Foreland Basins, Society for Sedimentary Geology, Special Publication, vol. 52, pp. 243–282.
Garrison Jr., J.R., Brinkman, D., Nichols, D.J., Layer, P., Burge, D., Thayn, D., 2007. A multidisciplinary study of the Lower Cretaceous Cedar Mountain Formation, Mussentuchit Wash, Utah: a determination of the paleoenvironment and paleoecology of the *Eolambia caroljonesa* dinosaur quarry. Cretaceous Research 28, 461–494.
Gaschnig, R.M., Vervoort, J.D., Lewis, R.S., McClelland, W.C., 2009. Migrating magmatism in the US cordillera: in situ U–Pb geochronology of the Idaho Batholith. Contributions to Mineral Petrology 159, 863–883.
Gehrels, G., Pecha, M., 2014. Detrital zircon U–Pb geochronology and Hf isotope geochemistry of Paleozoic and Triassic passive margin strata of western North America. Geosphere 10, 49–65.
Gerstenberger, H., Haase, G., 1997. A highly effective emitter substance for mass spectrometric Pb isotope ratio determinations. Chemical Geology 136, 309–312.
Gradstein, F., Ogg, J., 2004. Geologic time scale 2004 – why, how, and where next! Lethaia 37, 175–181.
Gradstein, F.M., Ogg, J.G., Smith, A.G., Bleeker, W., Lourens, L.J., 2004. A new geologic time scale, with special reference to Precambrian and Neogene. Episodes 27, 83–100.
Greenhalgh, B., Britt, B.B., 2007. Stratigraphy and sedimentology of the Morrison/Cedar Mountain formational boundary, east-central Utah. In: Willis, G.C., Hylland, M.D., Clark, D.L., Chidsey Jr., T.C. (Eds.), Central Utah – Diverse Geology of a Dynamic Landscape, Utah Geological Association Publication, vol. 36, pp. 81–100.
Guynn, J., Gehrels, G., 2010. Comparison of Detrital Zircon Age Distributions Using the K-S Test. Arizona LaserChron Center, University of Arizona, Tucson, Arizona.
Hay, W.W., Floegel, S., 2012. New thoughts about the Cretaceous climate and oceans. Earth-Science Reviews 115, 262–272.
Harries, P.J., Little, C.T., 1999. The early Toarcian (Early Jurassic) and the Cenomanian– Turonian (Late Cretaceous) mass extinctions: similarities and contrasts. Palaeogeography, Palaeoclimatology, Palaeoecology 154, 39–66.
Hunt, G.J., Lawton, T.F., Kirkland, J.I., Sprinkel, D.A., Yonkee, W.A., Chidsey, T.C., 2011. Detrital zircon U-Pb geochronological provenance of Lower Cretaceous strata, foreland basin, Utah. In: Sevier Thrust Belt: Northern and Central Utah and Adjacent Areas. Utah Geological Association Publication, vol. 40, pp. 193–211.
Jaffey, A.H., Flynn, K.F., Glendenin, L.E., Bentley, W.C., Essling, A.M., 1971. Precision measurements of half-lives and specific activities of ^{235}U and ^{238}U. Physical Review C 4, 1889–1906.
Jenkyns, H.C., 1980. Cretaceous anoxic events: from continents to oceans. Journal of the Geological Society 137 (2), 171–188.
Jones, M.M., Sageman, B.B., Meyers, S.R., 2018. Turonian sea level and paleoclimatic events in astronomically tuned records from the Tropical North Atlantic and Western Interior Seaway. Paleoceanography and Paleoclimatology 33, 470–492.
Jones, M.M., Sageman, B.B., Oakes, R.L., Parker, A.L., Leckie, R.M., Bralower, T.J., Sepúlveda, J., Fortiz, V., 2019. Astronomical Pacing of Relative Sea Level During Oceanic Anoxic Event 2: Preliminary Studies of the Expanded SH# 1 Core, vol. 131. Geological Society of America Bulletin, Utah, USA, pp. 1702–1722.
Jones, M.M., Sageman, B.B., Selby, D., Jicha, B.R., Singer, B.S., Titus, A.L., 2021. Regional chronostratigraphic synthesis of the Cenomanian-Turonian Oceanic Anoxic Event 2 (OAE2) interval, Western Interior Basin (USA): New Re-Os chemostratigraphy and ^{40}Ar/^{39}Ar geochronology. The Geological Society of America Bulletin 133, 1090–1104.
Joo, Y.J., Sageman, B.B., 2014. Cenomanian to Campanian carbon isotope chemostratigraphy from the Western Interior Basin, USA. Journal of Sedimentary Open-file report 597 Research 84, 529–542.
Joyce, W.G., Lyson, T.R., Kirkland, J.I., 2016. An early bothremydid (Testudines, Pleurodira) from the Late Cretaceous (Cenomanian) of Utah, North America. PeerJ 4, e2502. https://doi.org/10.7717/peerj.2502.
Kauffman, E.G., 1977. Geological and biological overview: Western Interior Cretaceous basin. In: Kauffman, E.G. (Ed.), Cretaceous Facies, Faunas, and Paleoenvironments Across the Western Interior Basin, The Mountain Geologist, vol. 14, pp. 75–99.
Kauffman, E.G., Caldwell, W.G.E., 1993. The Western Interior Basin in space and time. In: Caldwell, W.G.E., Kauffman, E.G. (Eds.), Evolution of the Western Interior Basin, Geological Association of Canada Special Paper, vol. 39, pp. 1–30.
Kauffman, E.G., Sageman, B.B., Kirkland, J.J., Elder, W.P., Harries, P.J., Villamil, T., 1993. Molluscan biostratigraphy of the Cretaceous Western Interior Basin, North America. In: Caldwell, W.G.E., Kauffman, E.G. (Eds.), Evolution of the Western Interior Basin, Geological Association of Canada Special Paper, vol. 39, pp. 397–434.
Keller, G., Berner, Z., Adatte, T., Stueben, D., 2004. Cenomanian–Turonian and δ13C, and δ18O, sea level and salinity variations at Pueblo, Colorado. Palaeogeography, Palaeoclimatology, Palaeoecology 211, 19–43.
Kennedy, W.J., Walaszczyk, I., Cobban, W.A., 2005. The global boundary stratotype section and point for the base of the Turonian stage of the Cretaceous: Pueblo, Colorado, USA. Episodes-Newsmagazine of the International Union of Geological Sciences 28, 93–104.
Kirkland, J.I., 1991. Lithostratigraphic and biostratigraphic framework for the Mancos Shale (Late Cenomanian to Middle Turonian) at Black Mesa, northeastern Arizona. In: Nations, J.D., Eaton, J.G. (Eds.), Stratigraphy, Depositional Environments, and Sedimentary Tectonics of the Western Margin, Cretaceous Western Interior Seaway, Geological Society of America Special Paper, vol. 260, pp. 85–111.
Kirkland, J.I., Suarez, M., Suarez, C., Hunt-Foster, R., 2016. The Lower Cretaceous in East- Central Utah-The Cedar Mountain Formation and its Bounding Strata. Geology of the Intermountain West 3, 101–228.
Kirschbaum, M.A., Schenk, C.J., 2010. Sedimentology and Reservoir Heterogeneity of a Valley-fill Deposit – A Field Guide to the Dakota Sandstone of the San Rafael Swell, Utah. United States Geological Survey 2010-5222, p. 36.
Kowallis, B.J., Christiansen, E.H., Deino, A., 1989. Multi-characteristic Correlation of Upper Cretaceous Volcanic Ash Beds From Southwestern Utah to Central Colorado. In: Utah Geological and Mineral Survey, Miscellaneous Publication, vol. 89, p. 22.
Kowallis, B.J., Christiansen, E.H., Deino, A.L., Kunk, M.J., Heaman, L.M., 1995. Age of the Cenomanian-Turonian boundary in the Western Interior of the United States. Cretaceous Research 16, 109–129.
Krogh, T.E., 1973. A low contamination method for hydrothermal decomposition of zircon and extraction of U and Pb for isotopic age determination. Geochimica et Cosmochimica Acta 37, 485–494.
Kuiper, K.F., Deino, A., Hilgen, F.J., Krijgsman, W., Renne, P.R., Wijbrans, A.J., 2008. Synchronizing rock clocks of Earth history. Science 320, 500–504.
Laskowski, A.K., DeCelles, P.G., Gehrels, G.E., 2013. Detrital zircon geochronology of Cordilleran retroarc foreland basin strata, western North America. Tectonics 32, 1027–1048.
Laurin, J., Sageman, B.B., 2007. Cenomanian–Turonian coastal record in SW Utah, USA: orbital-scale transgressive-regressive events during Oceanic Anoxic Event II. Journal of Sedimentary Research 77, 731–756.
Laurin, J., Barclay, R.S., Sageman, B.B., Dawson, R.R., Pagani, M., Schmitz, M., Eaton, J., McInerney, F.A., McElwain, J.C., 2019. Terrestrial and marginal-marine record of the mid-Cretaceous Oceanic Anoxic Event 2 (OAE 2): High-resolution framework, carbon isotopes, CO_2 and sea-level change. Palaeogeography, Palaeoclimatology, Palaeoecology 524, 118–136.
Lawton, T.F., Hunt, G.J., Gehrels, G.E., 2010. Detrital zircon record of thrust belt unroofing in Lower Cretaceous synorogenic conglomerates, central Utah. Geology 38, 463–466.
Leckie, R.M., Yuretich, R., West, O.L.O., Finkelstein, D., Schmidt, M.G., Dean, W.E., Arthur, M.A., 1998. Stratigraphy and Paleoenvironments of the Cretaceous Western Interior Seaway, USA. In: Dean, W.E., Arthur, M.A. (Eds.), Stratigraphy and Paleoenvironments of the Cretaceous Western Interior Seaway, USA, Society for Economic Paleontologists and Mineralogists, Concepts in Sedimentology and Paleontology, vol. 6, pp. 101–126.
Leithold, E.L., 1993. Preservation of laminated shale in ancient clinoforms: comparison to modern subaqueous deltas. Geology 21, 359–362.
Leithold, E.L., 1994. Stratigraphical architecture at the muddy margin of the Cretaceous Western Interior Seaway, southern Utah. Sedimentology 41, 521–543.

Leithold, E.L., Dean, W.E., 1998. Depositional processes and carbon burial on a Turonian prodelta at the margin of the Western Interior Seaway. Concepts in Sedimentology and Paleontology 6, 189–200.
Li, Z., Schieber, J., 2018. Detailed facies analysis of the Upper Cretaceous Tununk Shale Member, Henry Mountains Region, Utah: implications for mudstone depositional models in epicontinental seas. Sedimentary Geology 364, 141–159.
Li, Z., Schieber, J., 2020. Application of sequence stratigraphic concepts to the Upper Cretaceous Tununk Shale Member of the Mancos Shale Formation, south-central Utah: parasequence styles in shelfal mudstone strata. Sedimentology 67, 118–151.
Linde, G.M., Trexler Jr., J.H., Cashman, P.H., Gehrels, G., Dickinson, W.R., 2016. Detrital zircon U-Pb geochronology and Hf isotope geochemistry of the Roberts Mountains allochthon: New insights into the early Paleozoic tectonics of western North America. Geosphere 12, 1016–1031.
Lockley, M., Burton, R., Grondel, L., 2018. A large assemblage of tetrapod tracks from the Cretaceous Naturita Formation, Cedar Canyon region, southwestern Utah. Cretaceous Research 92, 108–121.
Londry, K.L., Des Marais, D.J., 2003. Stable carbon isotope fractionation by sulfate-reducing bacteria. Applied and Environmental Microbiology 69, 2942–2949.
Lowery, C.M., Leckie, R.M., 2017. Biostratigraphy of the Cenomanian–Turonian Eagle Ford Shale of south Texas. Journal of Foraminiferal Research 47, 105–128.
Lowery, C.M., Leckie, R.M., Bryant, R., Elderbak, K., Parker, A., Polyak, D.E., Schmidt, M., Snoeyenbos-West, O., Sterzinar, E., 2018. The Late Cretaceous Western Interior Seaway as a model for oxygenation change in epicontinental restricted basins. Earth-Science Reviews 177, 545–564.
Ludwig, K.R., 2003. User's Manual for Isoplot 3.00. Berkeley Geochronology Center, Berkeley, California.
Mantell, G.A., 1822. The Fossils of the South Downs; or Illustrations of the Geology of Sussex. Lupton Relfe, London, xvi +, p. 327.
Mattinson, J.M., 2005. Zircon U-Pb chemical abrasion ("CA-TIMS") method: combined annealing and multi-step partial dissolution analysis for improved precision and accuracy of zircon ages. Chemical Geology 220, 47–66.
Merewether, E.A., Cobban, W.A., Obradovich, J.D., 2011. Biostratigraphic Data From Upper Cretaceous formations-Eastern Wyoming, Central Colorado, and Northeastern New Mexico. In: United States Geological Survey, Scientific Investigations Map, vol. 3175, p. 10.
Meyers, S.R., Sageman, B., Hinnov, L., 2001. Integrated quantitative stratigraphy of the Cenomanian-Turonian Bridge Creek Limestone Member using evolutive harmonic analysis and stratigraphic modeling. Journal of Sedimentary Research 71, 628–643. https://doi.org/10.1306/012401710628.
Meyers, S.R., Sageman, B.B., Lyons, T., 2005. Organic carbon burial rate and the molybdenum proxy: Theoretical framework and application to Cenomanian-Turonian OAE II. Paleoceanography 20, PA2002. https://doi.org/10.1029/2004PA001068.
Meyers, S.R., Siewert, S.E., Singer, B.S., Sageman, B.B., Condon, D.J., Obradovich, J.D., Jicha, B.R., Sawyer, D.A., 2012. Intercalibration of radioisotopic and astrochronologic time scales for the Cenomanian-Turonian boundary interval, Western Interior Basin, USA. Geology 40, 7–10.
Miall, A.,D., Catuneanu, O., 2019. Chapter 9: The Western Interior Basin. In: Miall, A.D. (Ed.), The Sedimentary Basins of the United States and Canada. Elsevier, Amsterdam, pp. 401–443.
Miall, A.D., Catuneanu, O., Vakarelov, B.K., Post, R., 2008. The Western Interior Basin. Sedimentary basins of the world 5, 329–362.
Molenaar, C.M., Cobban, W.A., 1991. Middle Cretaceous Stratigraphy on the south and east side of the Uinta Basin, Northeastern Utah and Northwestern Colorado. In: United States Geological Survey Bulletin, Evolution of Sedimentary basins-Uinta and Piceance Basins 1787-P, p. 42.
Molenaar, C.M., Wilson, B.W., 1990. The Frontier Formation and Associated Rocks of Northeastern Utah and Northwestern Colorado. In: United States Geological Survey Bulletin 1787-M, p. 21.
Nesbitt, S.J., Denton, R.K., Loewen, M.A., Brusatte, S.L., Smith, N.D., Turner, A.H., Kirkland, J.I., McDonald, A.T., Wolfe, D.G., 2019. A mid-Cretaceous tyrannosauroid and the origin of North American end-Cretaceous dinosaur assemblages. Nature Ecology and Evolution 3, 892–899.
Obradovich, J.D., 1993. A Cretaceous Time Scale. In: Geological Association of Canada Special Paper, vol. 39, pp. 379–396.
O' Connor, L.K., Jenkyns, H.C., Robinson, S.A., Remmelzwaal, S.R., Batenburg, S.J., Parkinson, I.J., Gale, A.S., 2020. A re-evaluation of the Plenus Cold Event, and the links between CO_2, temperature, and seawater chemistry during OAE 2. Paleoceanography and Paleoclimatology 35, e2019PA003631. https://doi.org/10.1029/2019PA003631.
Ogg, J.G., Hinnov, L.A., 2012. Cretaceous. In: Gradstein, F.M., Ogg, J.G., Schmitz, M.D., Ogg, G.M. (Eds.), The Geologic Time Scale 2012. Elsevier, Boston, Massachusetts, pp. 793–853.
Pecha, M.E., Gehrels, G.E., Karlstrom, K.E., Dickinson, W.R., Donahue, M.S., Gonzales, D.A., Blum, M.D., 2018. Provenance of Cretaceous through Eocene strata of the Four Corners region: Insights from detrital zircons in the San Juan Basin, New Mexico and Colorado. Geosphere 14, 785–811.
Phillips, S.P., Howell, J.A., Hartley, A.J., Chmielewska, M., 2020. Tidal estuarine deposits of the transgressive Naturita Formation (Dakota Sandstone): San Rafael Swell, Utah, USA. Journal of Sedimentary Research 90, 777–795.
Pratt, L.M., Threlkeld, C.N., 1984. Stratigraphic significance of $^{13}C/^{12}C$ ratios in mid-Cretaceous rocks of the Western Interior, U.S.A. In: Stott, D.F., Glass, D.J. (Eds.), The Mesozoic of Middle North America, Canadian Society of Petroleum Geologists, vol. 9, pp. 305–312.
Quinn, G.M., Hubbard, S.M., Putnam, P.E., Matthews, W.A., Daniels, B.G., Guest, B., 2018. A Late Jurassic to Early Cretaceous record of orogenic wedge evolution in the Western Interior Basin, USA and Canada. Geosphere 14, 1187–1206.
Rigby, J.K., Russon, M.P., Carroll, R.E., 1987. The Book Cliffs Cretaceous Section: Western edge of the Interior Seaway. In: Geological Society of America Centennial Field Guide, pp. 251–256.
Roca, X., Nadon, G.C., 2007. Tectonic control on the sequence stratigraphy of nonmarine retroarc foreland basin fills: insights from the Upper Jurassic of central Utah, USA. Journal of Sedimentary Research 77, 239–255.
Rossignol, C., Hallot, E., Bourquin, S., Poujol, M., Jolivet, M., Pellenard, P., Ducassou, C., Nalpas, T., Heilbronn, G., Yu, J., Dabard, M.P., 2019. Using volcaniclastic rocks to constrain sedimentation ages: to what extent are volcanism and sedimentation synchronous? Sedimentary Geology 381, 46–64.
Ryer, T.A., Phillips, R.E., Bohor, B.F., Pollastro, R.M., 1980. Use of altered volcanic ash falls in stratigraphic studies of coal-bearing sequences: an example from the Upper Cretaceous Ferron Sandstone Member of the Mancos Shale in central Utah. The Geological Society of America Bulletin 91, 579–586.
Sageman, B.B., Rich, J., Arthur, M.A., Birchfield, G.E., Dean, W.E., 1997. Evidence for Milankovitch periodicities in Cenomanian-Turonian lithologic and geochemical cycles, Western Interior USA. Journal of Sedimentary Research 67 (2), 286–302.
Sageman, B.B., Meyers, S.R., Arthur, M.A., 2006. Orbital time scale and new C-isotope record for Cenomanian-Turonian boundary stratotype. Geology 34, 125–128.
Santos, J.S., Kurek, M., Fouskas, F., 2017. Midwest Geobiology Symposium. http://www.midwestgeobiology.org/programs/MWGB2017.pdf.
Sauer, K.B., Gordon, S.M., Miller, R.B., Vervoort, J.D., Fisher, C.M., 2017. Evolution of the Jura-Cretaceous North American Cordilleran margin: insights from detrital-zircon U-Pb and Hf isotopes of sedimentary units of the North Cascades Range, Washington. Geosphere 13, 2094–2118.
Schlanger, S.O., Jenkyns, H.C., 1976. Cretaceous oceanic anoxic events: causes and consequences. Geologie en Mijnbouw 55, 3–4.
Schmitz, M.D., Schoene, B., 2007. Derivation of isotope ratios, errors and error correlations for U–Pb geochronology using ^{205}Pb-^{235}U-(^{233}U)-spiked isotope dilution thermal ionization mass spectrometric data. Geochemistry, Geophysics, Geosystems 8, Q08006.
Scholle, P.A., Arthur, M.A., 1980. Carbon isotope fluctuations in Cretaceous pelagic limestones: potential stratigraphic and petroleum exploration tool. AAPG Bulletin 64 (1), 67–87.
Seitz, O., 1934. Die Variabilität des *Inoceramus labiatus* v. Schlotheim. Jahrbuch der Königlichen Preußischen Geologischen Landesanstalt 55, 426, 274.
Sethi, P.S., Leithold, E.L., 1997. Recurrent depletion of benthic oxygen with 4th-order transgressive maxima in the Cretaceous Western Interior Seaway. Palaeogeography, Palaeoclimatology, Palaeoecology 128, 39–61.
Shumard, B.F., 1860. Descriptions of new Cretaceous fossils from Texas. Academy Science St Louis Transactions 1, 590–610.
Singer, B.S., Jicha, B.R., Sawyer, D., Walaszczyk, I., Buchwaldt, R., Mutterlose, J., 2020. Geochronology of Late Albian-Cenomanian Strata in the US Western Interior. Geological Society of America Bulletin.
Sláma, J., Košler, J., Condon, D.J., Crowley, J.L., Gerdes, A., Hanchar, J.M., Horstwood, M.S.A., Morris, G.A., Nasdala, L., Norberg, N., Schaltegger, U., Schoene, B., Tubrett, M.N., Whitehouse, M.J., 2008. Plešovice zircon-a new natural reference material for U–Pb and Hf isotopic microanalysis. Chemical Geology 241, 1–35.
Sowerby, J. de C., 1829. The mineral conchology of Great Britain, vol. 6. B. Meredith, London, pp. 504–609.
Sprinkel, D.A., Madsen, S.K., Kirkland, J.I., Waanders, G.L., Hunt, G.I., 2012. Cedar Mountain and Dakota formations around Dinosaur National Monument: Evidence of the incursion of the Cretaceous Western Interior Seaway into Utah. Utah Geological Survey Special Study 143, 1–20.
Stangroom, A.M., 2012. High-precision U/Pb dating of the Cenomanian-Turonian boundary Kaiparowits Plateau, Utah (Unpubl. Ph.D. thesis). Massachusetts Institute of Technology, Cambridge, Massachusetts, p. 40.
Stanton, T.W., 1893. The Colorado formation and its invertebrate fauna. Bulletin of the United States Geological Survey 106, 1–288.
Suarez, C.A., González, L.A., Ludvigson, G.A., Cifelli, R.L., Tremain, E., 2012. Water utilization of the Cretaceous Mussentuchit Member local vertebrate fauna, Cedar Mountain Formation, Utah, USA: using oxygen isotopic composition of phosphate. Palaeogeography, Palaeoclimatology, Palaeoecology 313, 78–92.
Szwarc, T.S., Johnson, C.L., Stright, L.E., McFarlane, C.M., 2015. Interactions between axial and transverse drainage systems in the Late Cretaceous Cordilleran foreland basin: evidence from detrital zircons in the Straight Cliffs Formation, southern Utah, USA. Bulletin of the Geological Society of America 127, 372–392.
Tibert, N.E., Leckie, R.M., 2013. Cenomanian-Turonian (Upper Cretaceous) foraminifera from the westernmost Colorado Plateau. Micropaleontology, southwest Utah, USA, pp. 555–578.
Tibert, N.E., Leckie, R.M., Eaton, J.G., Kirkland, J.I., Colin, J.-P., Leithold, E.L., McCormic, M., 2003. Recognition of relative sea level change in upper Cretaceous coal-bearing strata: A paleoecological approach using agglutinated foraminifera and ostracodes to detect key stratigraphic surfaces. In: Olson, H., Leckie, R.M. (Eds.), Microfossils as Proxies for Sea Level Change and Stratigraphic Discontinuities, Society for Sedimentary Geology Special Publication, vol. 75, pp. 263–299.
Tsikos, H., Jenkyns, H.C., Walsworth-Bell, B., Petrizzo, M.R., Forster, A., Kolonic, S., Erba, E., Silva, I.P., Baas, M., Wagner, T., Damsté, J.S., 2004. Carbon-isotope

stratigraphy recorded by the Cenomanian–Turonian Oceanic Anoxic Event: correlation and implications based on three key localities. Journal of the Geological Society 161, 711–719.
Tucker, R.T., Suarez, C.A., Makovicky, P.J., Zanno, L.E., 2022. Paralic sedimentology of the Mussentuchit Member Coastal Plain Cedar Mountain Formation, Central Utah. Journal of Sedimentary Research 92 (6), 546–569.
Tucker, R.T., Zanno, L.E., Huang, H.Q., Makovicky, P.J., 2020. A refined temporal framework for newly discovered fossil assemblages of the upper Cedar Mountain Formation (Mussentuchit Member), Mussentuchit Wash, Central Utah. Cretaceous Research 110, 104384. https://doi.org/10.1016/j.cretres.2020.104384.
Turgeon, S.C., Creaser, R.A., 2008. Cretaceous oceanic anoxic event 2 triggered by a massive magmatic episode. Nature 454, 323–326.
van Helmond, N.A.G.M., Sluijs, A., Sinninghe Damsté, J.S., Reichart, G.J., Voigt, S., Erbacher, J., Pross, J., Brinkhuis, H., 2015. Freshwater discharge controlled deposition of Cenomanian–Turonian black shales on the NW European epicontinental shelf (Wunstorf, northern Germany). Climate of the Past 11, 495–508.
van Helmond, N.A., Sluijs, A., Papadomanolaki, N.M., Plint, A.G., Gröcke, D.R., Pearce, M.A., Eldrett, J.S., Trabucho-Alexandre, J., Walaszczyk, I., Schootbrugge, B.V.D., Brinkhuis, H., 2016. Equatorward phytoplankton migration during a cold spell within the Late Cretaceous super-greenhouse. Biogeosciences 13, 2859–2872.
Walaszczyk, I., Shank, J.A., Plint, A.G., Cobban, W.A., 2014. Interregional correlation of disconformities in Upper Cretaceous strata, Western Interior Seaway: Biostratigraphic and sequence-stratigraphic evidence for eustatic change. Bulletin of the Geological Society of America 126, 307–316.
Warren, P.S., Stelck, C.R., 1969. Early *Neogastroplites,* Fort St. John Group, Western Canada. Bulletin of Canadian Petroleum Geology 17, 529–547.
Watkins, D.K., Bralower, T.J., Covington, J.M., Fisher, C.G., 1993. Biostratigraphy and paleoecology of the Upper Cretaceous calcareous nannofossils in the Western Interior Basin, North America. In: Caldwell, W.G.E., Kauffman, E.G. (Eds.), Evolution of the Western Interior Basin: Geological Association of Canada Special Paper, vol. 39, pp. 521–537.
Watson, E.B., Wark, D.A., Thomas, J.B., 2006. Crystallization thermometers for zircon and rutile. Contributions to Mineralogy and Petrology 15, 413–433.
White, T., Furlong, K., Arthur, M., 2002. Forebulge migration in the Cretaceous Western Interior basin of the central United States. Basin Research 14, 43–54.
Willis, G.C., 1999. The Utah thrust system – an overview. In: Spangler, L.E., Allen, C.J. (Eds.), Geology of Northern Utah and Vicinity, vol. 27. Utah Geological Association Publication, pp. 1–9.
Wright, C.W., Kennedy, W.J., 1981. The Ammonoidea of the Plenus Marls and the Middle Chalk. In: Monograph of the Palaeontographical Society, Publication, vol. 560, pp. 1–148 (part of Vol. 134 for 1980.
Young, R.G., 1960. Dakota Group of Colorado Plateau. American Association of Petroleum Geologists Bulletin 44, 156–194.
Young, R.G., 1965. Type section of Naturita Formation. American Association of Petroleum Geologists Bulletin 49, 1512–1516.
Zanno, L.E., Tucker, R.T., Canoville, A., Avrahami, H.M., Gates, T.A., Makovicky, P.J., 2019. Diminutive fleet-footed tyrannosauroid narrows the 70-million-year gap in the North American fossil record. Communications Biology 2, 1–12.
Zelt, F.B., 1985. Natural Gamma-ray Spectrometry, Lithofacies, and Depositional Environments of Selected Upper Cretaceous Marine Mudrocks, Western United States, Including Tropic Shale and Tununk Member of Mancos Shale (Unpubl. Ph.D. thesis). Princeton University, Princeton, New Jersey, p. 372.

Appendix A. Supplementary data

Supplementary data to this article can be found online at https://doi.org/10.1016/j.cretres.2022.105464.